EP2 AGONIST DID NOT INDUCE INFLAMMATION OF THE SYNOVIUM

It is important whether the EP2 agonist induced unfavorable inflammation during the regeneration process. We evaluated the synovium based on mRNA expression and histological scoring, and also measured the amounts of cytokines in joint fluid at 4 weeks. PGE2 was reported to up-regulate the expression of the *MMP3*, *TIMP3*, and *IL-1β* genes[3]. The expression of these inflammation-related genes was analyzed by semi-quantitative [Fig. 6(A)] and quantitative RT-PCR [Fig. 6(B)] using samples taken at 4 weeks. No significant up-regulation was found in either gene even in samples treated with a larger amount of EP2 agonist [Fig. 6(B)]. The activity of MMP3 in joint fluid had almost the same value as found in untreated joints [Fig. 6(C)]. The amount of TNF-α or CRP in treated knee joints showed no significant change compared with that in normal joints either [Fig. 6(D)]. Lining synovial cells showed no numerical or morphological change on treatment of with the agonist (400 μg/gel) [Fig. 6(E)], and the histological scoring for inflammation in the treated side was equal to that in the contralateral side [Fig. 6(F)]. These results

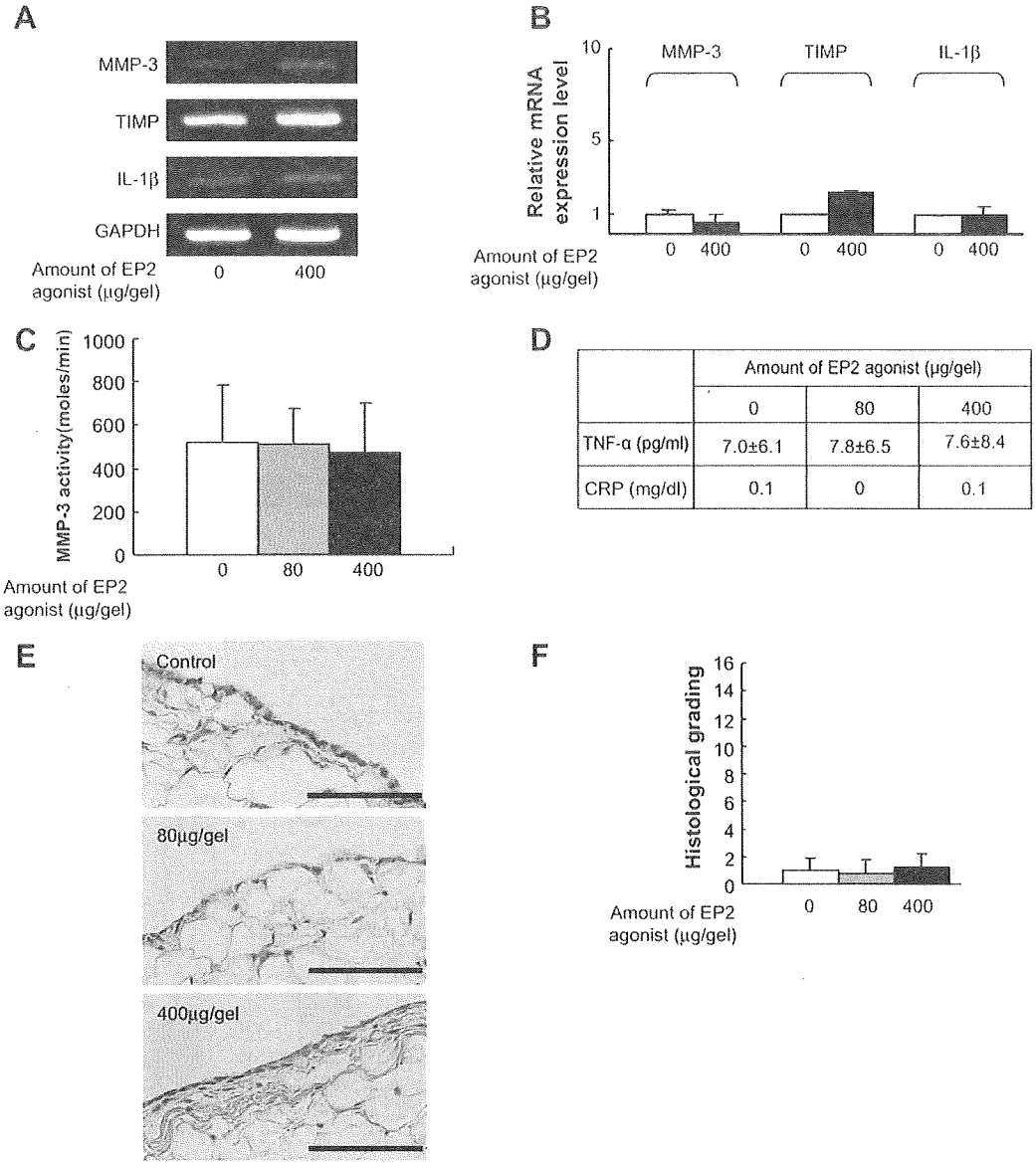

Fig. 6. EP2 agonist did not induce inflammation of the synovium. Inflammatory signs in knee joints were investigated in contralateral or EP2 agonist (80 or 400 μg/gel)-treated samples at 4 weeks after the operation in the osteochondral defect model. A and B: mRNA expression of inflammatory cytokines of cells in the synovium. RNA extracted from synovium was analyzed by semi-quantitative (A) and quantitative (B) RT-PCR. C: Activity of MMP3 in joint fluid. Joint fluid was collected from knee joints of contralateral (open square) and EP2 agonist-treated (blackened square) samples, and the activity of MMP3 was analyzed as described in the Materials and methods section. Five samples were analyzed in each group. D: Amount of TNF-α and CRP in joint fluid. Joint fluid was collected from five knee joints in each group. E: HE staining of synovium in knee joints. Specimens were prepared from a contralateral sample (a), and EP2 agonist-treated samples (b, 80 μg/gel; c, 400 μg/gel). Magnification 200×. Bar = 100 μm. F: Histological scoring of inflammation. Five specimens were analyzed in each of the contralateral and EP2 agonist-treated groups.

indicated that the EP2 agonist induced no significant inflammatory reaction in knee joints at the dose used in this study.

Discussion

PGE2 is a major prostanoid synthesized in response to various stimuli in a variety of cells and exerts local and systemic pleiotropic effects. In general, PGE2 plays a role in maintaining the physiological homeostasis, but in some pathogenic conditions such as inflammation and carcinogenesis, the excess PGE2 induced by factors such as inflammatory cytokines worsens the condition[10]. From this standpoint, PGE2 may be regarded as a pro-inflammatory factor promoting the pathological stage of OA. On the other hand, PGE2 has an anti-inflammatory function. Typical anti-inflammatory actions of PGE2 are demonstrated by the suppressive role of the PGE2 signal *via* EP3 in asthma[20]. As for the PGE2 signal *via* EP2, several reports have analyzed the relationship with inflammation. In human periodontal ligament cells, PGE2 signal *via* EP2/EP4 down-regulated the production of MMP3 and IL-6 stimulated by IL-1[21,22]. An EP4 agonist stimulated the production of MMP9 in macrophages, which was not observed on treatment with an EP2 agonist[23]. The expression of *COX-2* and *MMP9* genes was elevated in macrophages from EP2 null mice[24]. These results suggested that PGE2 acting through EP2 has a minimal role as a pro-inflammatory factor.

Our previous[11] and current study suggested that PGE2 signal *via* EP2 is not only anti-inflammatory but also promotes the regeneration of articular cartilage. The regeneration process of osteochondral defect may mimic the endochondral ossification in fracture healing, and several studies have already shown that the PGE2 signal involved in this process[25–28], among which signals *via* EP2 was particularly important[29]. Cells derived from bone marrow may play a central role in this process. On the other hand, the chondral defect model in this study may mimic the some stage of OA, in which cartilage tissue disappeared and subchondral bone was sclerosed. At this stage, the recruitment of bone marrow-derived cells was minimum, and, therefore, restoration of cartilage tissues was hardly observed. The therapeutic effects of EP2 agonist in this type of model, therefore, may be due to its effects directly on the remaining chondrocytes which are at the resting state in physiological condition as indicated by no PCNA staining [Fig. 3(A)]. The effects of EP2 agonist treatment were more prominent at the later time point (12 weeks) in both chondral and osteochondral defect models, suggesting that the regeneration of cartilage tissue was dependent on the growth of articular chondrocytes with low growth property. We observed that the amount of regenerated tissues was much less at 12 weeks than at 4 weeks after operation in control and contralateral samples, suggesting that regenerated cartilage tissues may lack the proper quality to maintain the structure, and the treatment with EP2 agonist may prevent such degeneration.

One of interesting finding in the current study is that the treatment with EP2 agonist enhanced the reconstruction of boundary between articular cartilage and subchondral bone, which is an important factor to maintain the articular structure. We have no clear explanation for this interesting phenomenon. As mentioned above, EP2 agonists stimulate the growth of both cartilage and bone marrow cells, which may relate to the physiological reconstruction of boundary.

It should be noted that the histological scale of contralateral samples tended to be better than that of control samples (Figs. 1 and 2) and the scales of contralateral samples of 400 μg/gel-treated animals were significantly better than 80 μg/gel-treated animals at 12 weeks [Fig. 2(D), $P = 0.02$], suggesting that there might be an effect from the treated-site through the systemic circulation. Although there were no signs of a general effect of PGE2 such as a reduction in blood pressure (data not shown), continuous release of the EP2 agonist may affect tissue regeneration on the contralateral side.

The ideal regeneration-promoting therapeutics will be small molecules which can be produced in a large amount, promote the regeneration of articular cartilage with a physiological structure, and have no adverse effects in other tissues either locally or systemically. No osteophyte formation was observed in any samples described in this study and also samples observed for a longer period (24 weeks) (data not shown). The results of this study suggested that the EP2 agonist is a promising candidate for such a new drug. Because EP4 is not expressed in normal articular chondrocytes[11], we have been focusing the analysis of EP2 agonist. In the case of osteochondral defect model, however, the combination of EP2/EP4 agonist is a reasonable choice to test considering the fact that the simultaneous activation of EP2 and EP4 cooperatively induced type II collagen mRNA expression[7]. The current experimental model has been used in several prior investigations of various articular repair procedures[30], but may not reflect the pathogenesis of OA (no mechanical factor, no inflammation, no aging factor). Further confirmation of the effect of EP2 agonists in combination with a more effective drug delivery system and experimental OA models in larger animals may lead to a new way to treat OA.

Conflict of interest

The authors declare that they have no conflict of interest.

Acknowledgments

We are grateful to Drs H. Ito, H. Yoshitomi, K. Nishitani, and B. Liang for providing helpful suggestions. This work was supported by Grants-in-aid for Scientific Research from the Japan Society for the Promotion of Science, from the Ministry of Education, Culture, Sports, Science, and Technology, and from the Ministry of Health, Labor, and Welfare.

Supplementary material

Supplementary material for this article may be found, in the online version, at doi: 10.1016/j.joca.2008.09.003.

References

1. Goldring MB, Goldring SR. Osteoarthritis. J Cell Physiol 2007;213: 626–34.
2. Goldring SR, Goldring MB. The role of cytokines in cartilage matrix degeneration in osteoarthritis. Clin Orthop Relat Res 2004;(427 Suppl):S27–36.
3. Martel-Pelletier J, Pelletier JP, Fahmi H. Cyclooxygenase-2 and prostaglandins in articular tissues. Semin Arthritis Rheum 2003;33:155–67.
4. Bunning RA, Russell RG. The effect of tumor necrosis factor alpha and gamma-interferon on the resorption of human articular cartilage and on the production of prostaglandin E and of caseinase activity by human articular chondrocytes. Arthritis Rheum 1989;32:780–4.
5. Miwa M, Saura R, Hirata S, Hayashi Y, Mizuno K, Itoh H. Induction of apoptosis in bovine articular chondrocyte by prostaglandin E(2) through cAMP-dependent pathway. Osteoarthritis Cartilage 2000;8: 17–24.

6. Riquet FB, Lai WF, Birkhead JR, Suen LF, Karsenty G, Goldring MB. Suppression of type I collagen gene expression by prostaglandins in fibroblasts is mediated at the transcriptional level. Mol Med 2000;6:705–19.
7. Miyamoto M, Ito H, Mukai S, Kobayashi T, Yamamoto H, Kobayashi M, *et al.* Simultaneous stimulation of EP2 and EP4 is essential to the effect of prostaglandin E2 in chondrocyte differentiation. Osteoarthritis Cartilage 2003;11:644–52.
8. Di Battista JA, Doré S, Morin N, He Y, Pelletier JP, Martel-Pelletier J. Prostaglandin E2 stimulates insulin-like growth factor binding protein-4 expression and synthesis in cultured human articular chondrocytes: possible mediation by Ca(++)-calmodulin regulated processes. J Cell Biochem 1997;65:408–19.
9. Lowe GN, Fu YH, McDougall S, Polendo R, Williams A, Benya PD, *et al.* Effects of prostaglandins on deoxyribonucleic acid and aggrecan synthesis in the RCJ 3.1C5.18 chondrocyte cell line: role of second messengers. Endocrinology 1996;137:2208–16.
10. Sugimoto Y, Narumiya S. Prostaglandin E receptors. J Biol Chem 2007; 282:11613–7.
11. Aoyama T, Liang B, Okamoto T, Matsusaki T, Nishijo K, Ishibe T, *et al.* PGE2 signal through EP2 promotes the growth of articular chondrocytes. J Bone Miner Res 2005;20:377–89.
12. Tani K, Naganawa A, Ishida A, Egashira H, Sagawa K, Harada H, *et al.* Design and synthesis of a highly selective EP2-receptor agonist. Bioorg Med Chem Lett 2001;11:2025–8.
13. Okada H. One- and three-month release injectable microspheres of the LH–RH superagonist leuprorelin acetate. Adv Drug Deliv Rev 1997; 28:43–70.
14. Katayama R, Wakitani S, Tsumaki N, Morita Y, Matsushita I, Gejo R, *et al.* Repair of articular cartilage defects in rabbits using CDMP1 gene-transfected autologous mesenchymal cells derived from bone marrow. Rheumatology (Oxford) 2004;43:980–5.
15. Yoshimi T, Kikuchi T, Obara T, Yamaguchi T, Sakakibara Y, Itoh H, *et al.* Effects of high-molecular-weight sodium hyaluronate on experimental osteoarthrosis induced by the resection of rabbit anterior cruciate ligament. Clin Orthop Relat Res 1994;298:296–304.
16. Fukuda T, Tani Y, Kobayashi T, Hirayama Y, Hino O. A new Western blotting method using polymer immunocomplexes: detection of Tsc1 and Tsc2 expression in various cultured cell lines. Anal Biochem 2000;285:274–6.
17. Qi C, Changlin H, Zefeng H. Matrix metalloproteinases and inhibitor in knee synovial fluid as cartilage biomarkers in rabbits: the effect of high-intensity jumping exercise. J Surg Res 2007;140:149–57.
18. Wu LD, Yu HC, Xiong Y, Feng J. Effect of dehydroepiandrosterone on cartilage and synovium of knee joints with osteoarthritis in rabbits. Rheumatol Int 2006;27:79–85.
19. Kawashima-Ohya Y, Satakeda H, Kuruta Y, Kawamoto T, Yan W, Akagawa Y, *et al.* Effects of parathyroid hormone (PTH) and PTH-related peptide on expressions of matrix metalloproteinase-2, -3, and -9 in growth plate chondrocyte cultures. Endocrinology 1998;139:2120–7.
20. Kunikata T, Yamane H, Segi E, Matsuoka T, Sugimoto Y, Tanaka S, *et al.* Suppression of allergic inflammation by the prostaglandin E receptor subtype EP3. Nat Immunol 2005;6:524–31.
21. Yan M, Noguchi K, Ruwanpura SM, Ishikawa I. Cyclooxygenase-2-dependent prostaglandin (PG) E2 downregulates matrix metalloproteinase-3 production *via* EP2/EP4 subtypes of PGE2 receptors in human periodontal ligament cells stimulated with interleukin-1alpha. J Periodontol 2005;76:929–35.
22. Noguchi K, Maeda M, Ruwanpura SM, Ishikawa I. Prostaglandin E2 (PGE2) downregulates interleukin (IL)-1alpha-induced IL-6 production *via* EP2/EP4 subtypes of PGE2 receptors in human periodontal ligament cells. Oral Dis 2005;11:157–62.
23. Tchetina EV, Di Battista JA, Zukor DJ, Antoniou J, Poole AR. Prostaglandin PGE2 at very low concentrations suppresses collagen cleavage in cultured human osteoarthritic articular cartilage: this involves a decrease in expression of proinflammatory genes, collagenases and COL10A1, a gene linked to chondrocyte hypertrophy. Arthritis Res Ther 2007;9:R75.
24. Pavlovic S, Du B, Sakamoto K, Khan KM, Natarajan C, Breyer RM, *et al.* Targeting prostaglandin E2 receptors as an alternative strategy to block cyclooxygenase-2-dependent extracellular matrix-induced matrix metalloproteinase-9 expression by macrophages. J Biol Chem 2006;281:3321–8.
25. Simon AM, Manigrasso MB, O'Connor JP. Cyclo-oxygenase 2 function is essential for bone fracture healing. J Bone Miner Res 2002;17: 963–76.
26. Gerstenfeld LC, Al-Ghawas M, Alkhiary YM, Cullinane DM, Krall EA, Fitch JL, *et al.* Selective and nonselective cyclooxygenase-2 inhibitors and experimental fracture-healing. Reversibility of effects after short-term treatment. J Bone Joint Surg Am 2007;89:114–25.
27. Einhorn TA. The science of fracture healing. J Orthop Trauma 2005; 19(10 Suppl):S4–6.
28. Yamakawa K, Kamekura S, Kawamura N, Saegusa M, Kamei D, Murakami M, *et al.* Association of microsomal prostaglandin E synthase 1 deficiency with impaired fracture healing, but not with bone loss or osteoarthritis, in mouse models of skeletal disorders. Arthritis Rheum 2008;58:172–83.
29. Paralkar VM, Borovecki F, Ke HZ, Cameron KO, Lefker B, Grasser WA, *et al.* An EP2 receptor-selective prostaglandin E2 agonist induces bone healing. Proc Natl Acad Sci U S A 2003; 100:6736–40.
30. Breinan HA, Hsu HP, Spector M. Chondral defects in animal models: effects of selected repair procedures in canines. Clin Orthop Relat Res 2001;(391 Suppl):S219–30.

TISSUE ENGINEERING: Part C
Volume 15, Number 00, 2009

DOI: 10.1089/ten.tec.2008.0693

A Novel Method to Isolate Mesenchymal Stem Cells from Bone Marrow in a Closed System Using a Device Made by Nonwoven Fabric

Kinya Ito, M.D.,[1,2] Tomoki Aoyama, M.D., Ph.D.,[1] Kenichi Fukiage, M.D.,[1,3] Seiji Otsuka, M.D., Ph.D.,[1,2] Moritoshi Furu, M.D.,[1,3] Yonghui Jin, M.D.,[1] Akira Nasu, M.D.,[1,3] Michiko Ueda,[1] Yasunari Kasai,[4] Eishi Ashihara, M.D., Ph.D.,[4] Shinya Kimura, M.D., Ph.D.,[4] Taira Maekawa, M.D., Ph.D.,[4] Akira Kobayashi, Ph.D.,[5] Shinya Yoshida, Ph.D.,[5] Hideo Niwa, Ph.D.,[5] Takanobu Otsuka, M.D., Ph.D.,[2] Takashi Nakamura, M.D., Ph.D.,[3] and Junya Toguchida, M.D., Ph.D.[1]

Bone marrow stromal cells (BMSCs) include cells with multidirectional differentiation potential described as mesenchymal stem cells. For clinical use, it is important to develop a way to isolate BMSCs from bone marrow in a closed system without centrifugation. After screening 200 biomaterials, we developed a device containing a nonwoven fabric filter composed of rayon and polyethylene. The filter selectively traps BMSCs among mononuclear cells in bone marrow based on affinity, not cell size. The cells are then recovered by the retrograde flow. Using canine and human bone marrow cells, the biological properties of BMSCs isolated by the device were compared with those obtained by conventional methods using centrifugation. The total number isolated by the device was larger, as was the number of $CD106^+/STRO\text{-}1^+$ double-positive cells. The cells showed osteogenic, chondrogenic, and adipogenic differentiation potential *in vitro*. Finally, the direct transplantation of cells isolated by the device without *in vitro* cultivation accelerated bone regeneration in a canine model of osteonecrosis *in vivo*. The proposed method is rapid and efficient, does not require a biological clean area, and will be useful for the clinical application of mesenchymal stem cells in bone marrow.

Introduction

BONE MARROW STROMAL CELLS (BMSCs) include cells with multidirectional differentiation potential such as mesenchymal stem cells (MSCs), multipotent adult progenitor cells, and marrow-isolated adult multilineage inducible cells, although it is not yet clear whether these cell types are distinct or overlap.[1,2] In spite of such ambiguity, BMSC-derived multipotent cells have been used in various fields of regenerative medicine. For clinical applications, however, it is critical to develop a method separating BMSCs containing multipotent cells from other types of cells in bone marrow that is simple, safe, inexpensive, and achievable in a closed system. The most popular way to isolate BMSCs is the density gradient method using a detergent such as sucrose[3] although the process is technically demanding and time consuming. Simple centrifugation with low gravity can also separate mononuclear cells (MNCs) from erythrocytes, and BMSCs can be selected through adherence to plastic dishes.[4] This method, however, still needs centrifugation, which makes it difficult to perform in a closed system, and therefore requires a biologically clean room.

To avoid the need for centrifugation, we have attempted to develop a device that can isolate BMSCs by filtration, and have selected nonwoven fabrics as biomaterials. Nonwoven fabrics are engineered materials that provide specific functions such as absorbency, liquid repellency, resilience, stretch, softness, strength, flame retardancy, washability, and cushioning.[5] As for clinical applications, nonwoven fabrics are used mainly for two purposes, as scaffolds and filters. A number of studies have used nonwoven fabrics as scaffolds for tissue regeneration.[5–7] The material and diameter of the fabric are important for cell attachment.[6,8] For example, polyethylene terephthalate with fibers 9.0 μm in diameter is ideal for the osteogenic differentiation of MSCs.[6] As filters, nonwoven fabrics have been used to sterilize medical materials.[9] Lymphocytapheresis is a form of treatment for patients with autoimmune diseases, in which lymphocytes in

[1]Institute for Frontier Medical Sciences, Kyoto University, Kyoto, Japan.
[2]Department of Orthopaedic Surgery, Graduate School of Medical Sciences, Nagoya City University, Nagoya, Japan.
[3]Department of Orthopaedic Surgery, Graduate School of Medicine, Kyoto University, Kyoto, Japan.
[4]Department of Transfusion Medicine and Cell Therapy, Kyoto University Hospital, Kyoto, Japan.
[5]Kaneka Co., Osaka, Japan.

peripheral blood are removed to reduce immunoreactions. To replace the centrifugation process in lymphocytapheresis, a filtration method using nonwoven fabrics has been developed.[10] The trapping effect is attributed to the affinity of the material for cells and the size of the material's fibers, with almost all leukocytes trapped when the fibers are less than 3 μm in diameter.[10,11]

As pure mechanical trapping based on cell size can damage cell membranes, we have tried to develop a filter that traps MSCs through affinity and here show that a new device composed of rayon–polyethylene nonwoven fabrics can isolate BMSCs from bone marrow aspirates, which contain cells compatible with multipotent cells *in vitro* and *in vivo*.

Materials and Methods

Screening of materials

The basic concept behind our approach is to trap BMSCs among bone marrow aspirates on a filter, and collect them using a retrograde flow (Fig. 1A). Biomaterials for the filter were screened based on microscopic structure (evenness), diameter (over 10 μm), weight (over 50 g/m^2), bio-safety, and availability (as the first screening). Potentially suitable biomaterials were further screened by conducting colony-forming unit (CFU) assays described later using swine bone marrow cells in three steps (as the second, third, and fourth screening; Supplemental Fig. S1, available online at www.liebertonline.com).

Electron microscopic analyses

After bone marrow had permeated through it, the filter was treated with 2.5 wt% glutaraldehyde in saline for 2 days at 4°C. The samples were dried by passing them through a series of graded-alcohol-saline solutions. Finally, the solution was changed to 100% t-butanol, and the samples were freeze-dried for 10 h at −5°C. The dried membranes were coated with gold–palladium and examined using a S-3000N scanning electron microscope (Hitachi, Tokyo, Japan).

Harvesting of bone marrow

Humans. Ten milliliters of bone marrow was taken from iliac crests of donors who received orthopedic operative procedures requiring autologous bone grafts from iliac crests. The donors had no history of concurrent illness or of medication that could affect bone metabolism. The Ethics Committee of the Faculty of Medicine, Kyoto University, approved the procedure, and informed consent was obtained from each donor according to the declaration of Helsinki.

Dogs. Ten milliliters of bone marrow was aspirated from iliac crests of male beagle dogs (10–13 kg) under intravenous anesthesia. The experiments with animals were approved by the institutional animal research committee, and performed according to the Guidelines for Animal Experiments of Kyoto University.

Preparation of MNCs

Human marrow samples were divided equally into three aliquots (3 mL each). One aliquot was applied to the device (method D), which had been saturated with saline. After washing the filter with 10 mL of saline, trapped cells were collected by a retrograde flow of the culture medium into a collection bag (Fig. 1A). The second aliquot was suspended in 5 mL of α-minimum essential medium GlutaMAX (Invitrogen, Carlsbad CA,) with 10% fetal bovine serum (Hyclone, South Logan, UT). The suspension was centrifuged at 1200 rpm for 5 min. The supernatant and the buffy coat were re-suspended in another tube with 5 mL of α-minimum essential medium GlutaMAX with 10% fetal bovine serum. This method is hereafter designated method S (simple centrifugation).[4,12] The final aliquot of bone marrow was fractionated by centrifugation over a density cushion using a Ficoll gradient (GE Healthcare Life Sciences, Piscataway, NJ), as described.[3] The interface layer was harvested and washed twice with 10 mL of Hank's buffer solution. This method is hereafter designated method F (Ficoll gradient).

Collection efficacy

Cells trapped on the filter and collected by retrograde flow in the collection bag were designated the collected fraction, and cells flowing through the filter into the flow-through bag were designated the flow-through fraction (Fig. 1A). Collection efficacy was determined as the ratio of the number of cells in each fraction to that in the applied bone marrow.

CFU assay

For the CFU assay, the MNCs were diluted and plated in 60-mm cell culture dishes at a density of 2.5×10^5 cells/dish and incubated for 14 days ($n = 3$). The cells were fixed with methanol and stained with a 0.05% crystal violet solution. We counted the number of colony with a diameter more than 4 mm.

Flow cytometry

Cells were stained at room temperature for 30 min with the following antibodies: CD10-phycoerythrin (PE), CD34-allophycocyanin (APC), CD45-peridinin chlorophyll protein (PerCP-Cy5.5), CD106-fluorescein isothiocyanate (FITC), CD166-PE (BD Biosciences, San Jose, CA), CD90-FITC (Beckman Coulter, Fullerton, CA), CD271-APC (Miltenyi Biotec, Bergisch Gladbach, Germany), and STRO-1-PE (Santa Cruz Biotechnology, Santa Cruz, CA). They were subsequently subjected to flow cytometry using a FACS Calibur instrument (BD Biosciences).

Induction of differentiation and histochemical evaluating

Differentiation was induced using the standard method.[13] The differentiation potential was evaluated as below.

- Osteogenic differentiation: Calcified nodules were evaluated by alizarin red staining, and calcium content was quantified.
- Adipogenic differentiation: Intracellular lipid droplets were stained with oil red-O, and the amount of triglyceride was quantified.
- Chondrogenic differentiation: Cartilage matrix was evaluated by alcian blue staining, and the amount of glycosaminoglycan was quantified.

These analyses were described previously.[14]

Reverse transcription–polymerase chain reaction

Total RNA was extracted using RNeasy Kit (Qiagen, Hilden, Germany). All reverse transcription reactions were

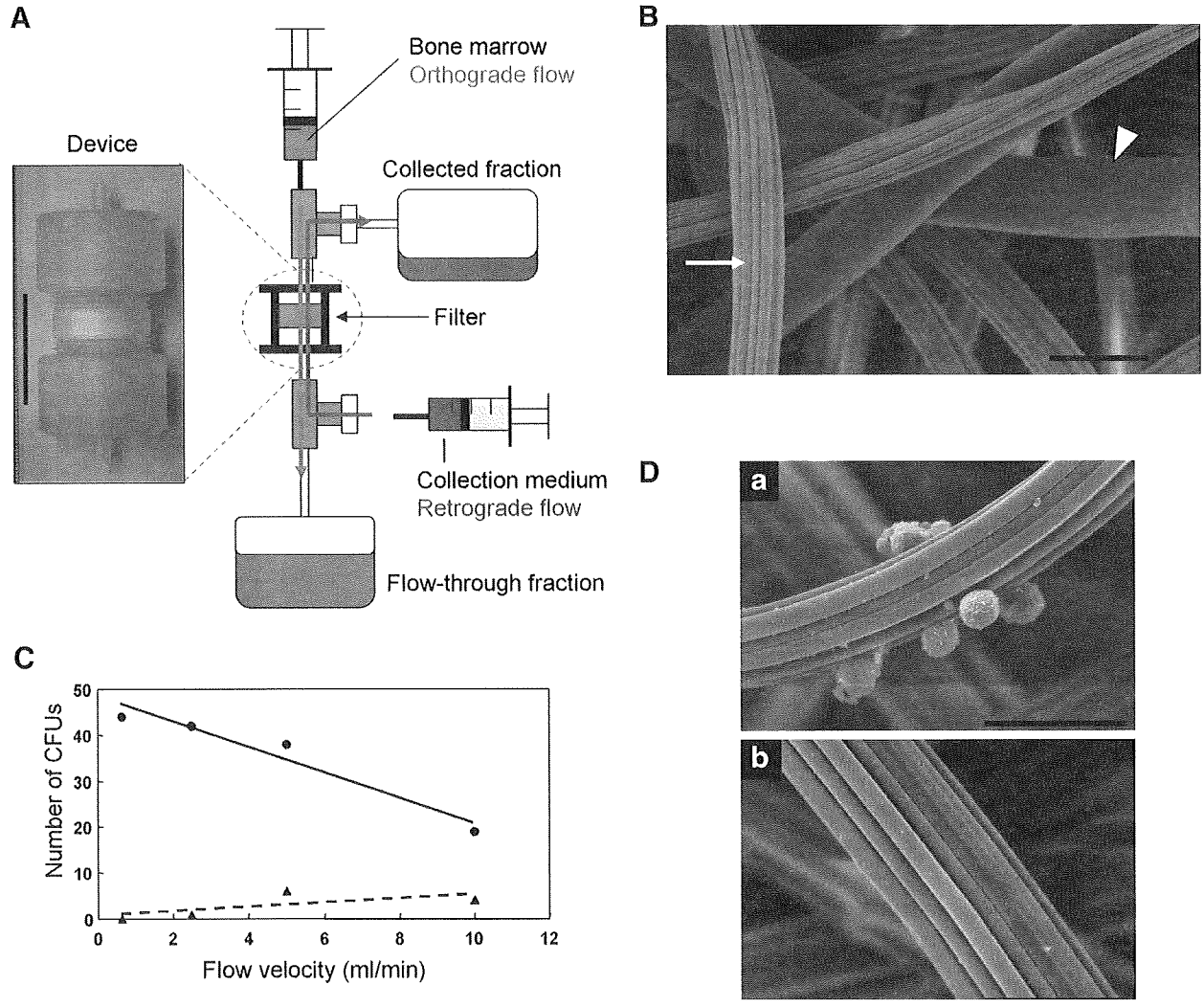

FIG. 1. Device containing a nonwoven fabric filter. (**A**) Photo of the device and schematic explanation of the collection method. The red line indicates the orthograde flow to apply bone marrow, and the blue line indicates the retrograde flow to collect cells. Scale bar = 30 mm. (**B**) Electron micrograph of the nonwoven fabric of rayon and polyethylene. Arrow, rayon; arrowhead, polyethylene. Magnification, 2000×. Scale bar = 20 μm. (**C**) Conditioning of flow velocity using swine bone marrow. Closed circles and closed triangles indicate the number of colony-forming units (CFUs) formed by cells in the collected fraction and flow-through fraction at the indicated flow velocity, respectively. (**D**) Electron micrograph of the surface of the filter after the orthograde flow of swine bone marrow (a) and after the retrograde flow of collection medium (b). Magnification, 2500×. Scale bar = 20 μm.

performed using the Super Script First Strand Synthesis System (Invitrogen). Polymerase chain reaction amplification was carried out using rTaq polymerase (Toyobo, Osaka, Japan). All polymerase chain reactions were performed using GeneAmp 9700 (PE Applied Biosystem, Foster City, CA) and specific primers for each gene.[14]

Preparation of the canine model of osteonecrosis and cell transplantation

A canine model of scapho-lunate osteonecrosis was prepared as described previously.[15] Briefly, scapho-lunates on one side were exposed dorsally, and a cortical window of 5×10 mm was made, through which as much cancerous bone as possible was removed. After the curettage, the cavity was filled with liquid nitrogen for 10 min, and the frozen bone was thawed at room temperature for 10 min. This freeze–thaw procedure was repeated three times. On one side, the bone cavity was filled with beta-tricalcium phosphate (β-TCP) granules (200 μg, 0.2 cm^3) (Osferion®; Olympus, Tokyo, Japan) (hereafter designated the control side). On the other side, canine BMSCs ($6.0\times10^7 \pm 1.5\times10^7$) isolated by the device from 10 mL of bone marrow were mixed with the same amount of β-TCP and transplanted into the bone cavity (hereafter designated the BMSC side). Finally, the bone window was plugged with 5×10 mm cortical bone. Animals were sacrificed and evaluated at 4 weeks after the operation ($n = 6$).

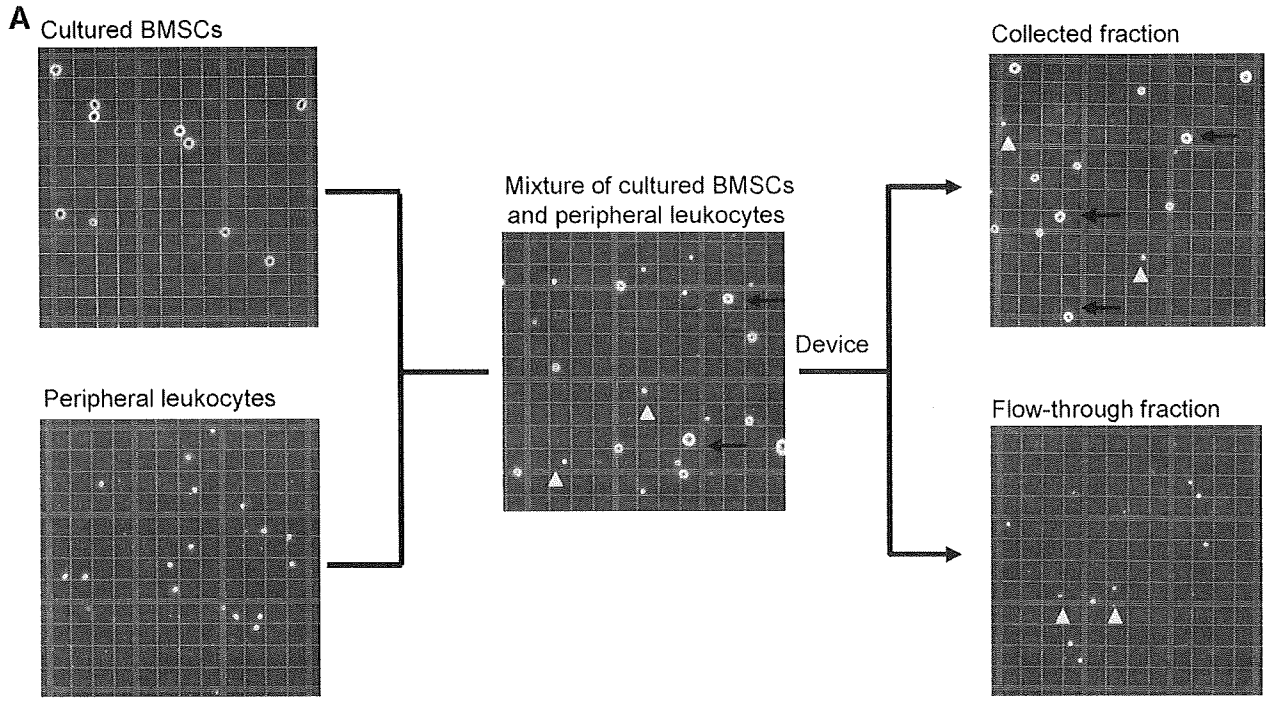
A
Cultured BMSCs
Peripheral leukocytes
Mixture of cultured BMSCs and peripheral leukocytes
Device
Collected fraction
Flow-through fraction

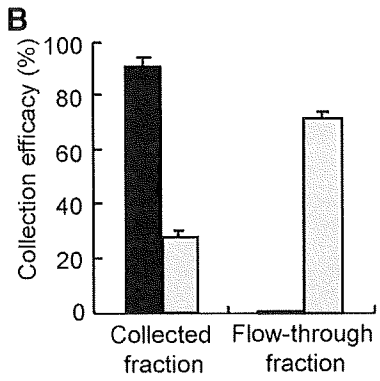
B
Collection efficacy (%)
100
80
60
40
20
0
Collected fraction
Flow-through fraction

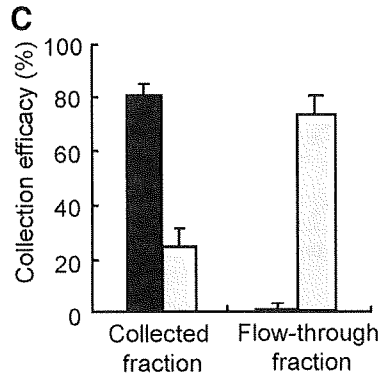
C
Collection efficacy (%)
100
80
60
40
20
0
Collected fraction
Flow-through fraction

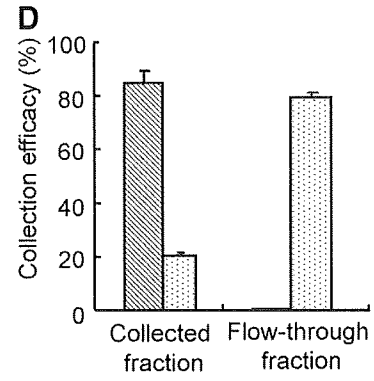
D
Collection efficacy (%)
100
80
60
40
20
0
Collected fraction
Flow-through fraction

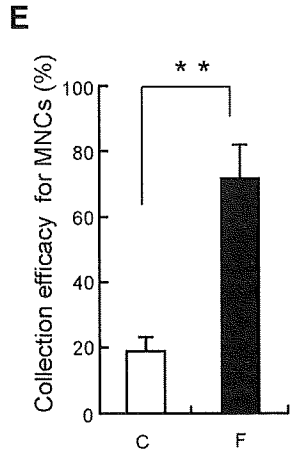
E
Collection efficacy for MNCs (%)
100
80
60
40
20
0
* *
C
F

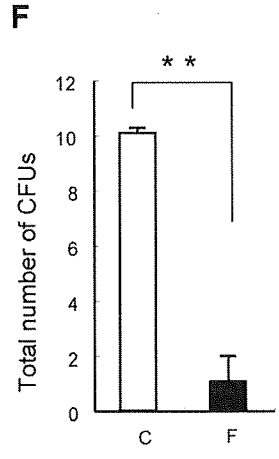
F
Total number of CFUs
12
10
8
6
4
2
0
* *
C
F

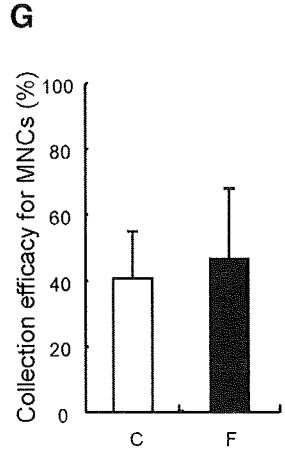
G
Collection efficacy for MNCs (%)
100
80
60
40
20
0
C
F

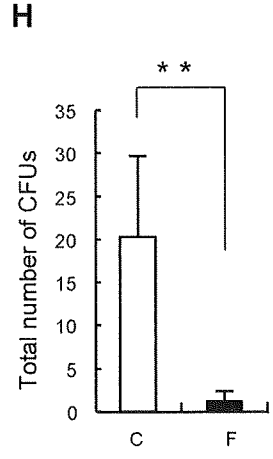
H
Total number of CFUs
35
30
25
20
15
10
5
0
* *
C
F

Imaging analyses

X-ray. Antero-posterior and lateral views of both wrists were obtained. The carpal height ratio was calculated from the antero-posterior view.[15,16] The Ståhl index was calculated from the lateral view.[15,17]

Micro-computed tomography. Canine carpal bones were scanned by computed tomography (CT) (SMX-100CT-SV3 type; Shimazu, Kyoto, Japan). The image consisted of 800 slices with a voxel size of 68.224 mm in all three axes. Coronal and sagittal cross-sectional views of the scapho-lunate were reconstructed using adjunctive software. The same setting was used for all samples. The image reconstruction and quantification of the scapho-lunate were performed with VG Studio MAX software (Nihon Visual Science, Tokyo, Japan).[15]

Macroscopic and microscopic assessments

The volume and weight of extracted scapho-lunate bones were actually measured using a scale. The samples were fixed in a 10% formalin solution, decalcified with Plank-Rychlo solution, and then embedded in paraffin. Serial sections were cut at 4 μm, and stained with hematoxylin–eosin and silver impregnation.

Using a light microscope, the absorption of β-TCP granules and the formation of bone were graded as follows.[18] For hematoxylin–eosin staining, granules were not surrounded by cells or newly forming bone (grade 1); granules were surrounded by osteoblasts and/or osteoclasts (grade 2); and granules were surrounded by newly forming bone (grade 3). For silver impregnation staining, granules were not completely surrounded by collagen fibrils (grade 1); granules were completely surrounded by collagen fibrils (grade 2); and granules were completely eroded with reticulated collagen fibrils (grade 3). All the β-TCP granules in a whole section were classified according to the three grades. The rates of each grade were then calculated.

Statistics

Results are expressed as the mean ± SE. The statistical analysis was first performed by the analysis of variance (ANOVA), and if there was a significant difference among samples, Turkey's *post hoc* test was performed for multiple comparisons. The Student's *t*-test was carried out to compare individual data. A significant difference was accepted at $p < 0.05$.

Results

Screening of materials

The first screening, of 200 potential biomaterials for the filter, was based on the parameters described in the Materials and Methods section. Forty materials were then selected for the second screening using swine bone marrow cells ($n = 2$). Ten biomaterials showed CFU counts of more than 10, and were selected for the third screening by CFU assay ($n = 3$), of which six preceded to the fourth and last screening ($n = 3$). Finally, a rayon–polyethylene nonwoven fabric was selected as the material for the filter (Supplemental Fig. S1, available online at www.liebertonline.com). First, the optimum velocity of filtration was determined by comparing CFU counts of cells in the collected and flow-through fractions. A velocity of 2.5 mL/min was chosen for further experiments (Fig. 1C). Electron microscopic analysis confirmed the binding of swine bone marrow cells and their detachment under retrograde flow (Fig. 1D, a and b).

Selective collection of BMSCs by the device

To analyze the device's selectivity, cultured human BMSCs or peripheral leukocytes were applied to it, and the cells in the collected fraction and flow-through fractions were enumerated (Fig. 2B). More than 90% of BMSCs were collected in the collected fraction, compared to only 28% of peripheral leukocytes (Fig. 2B). This selectivity was also observed when equal numbers (1×10^6) of BMSCs and peripheral leukocytes were mixed and then applied to the device (Fig. 2C). Because BMSCs and peripheral leukocytes differ in size, we could distinguish between them in the cell counting chamber (Fig. 2A). Approximately 80% of BMSCs were collected in the collected fraction, and an almost equal percentage of peripheral leukocytes were collected in the flow-through fraction (Fig. 2C). More than 90% of $CD44^+$ cells were collected with the device, leaving almost no $CD44^+$ cells in the flow-through fraction, whereas less than 20% of $CD45^+$ cells were collected (Fig. 2D). These results suggested the selective collection of BMSCs by the device.

FIG. 2. Selective collection of bone marrow stromal cells (BMSCs) with CFUs by the device. (**A**) Selective counting of BMSCs and peripheral leukocytes. BMSCs and peripheral leukocytes differed in morphology in the cell counting chamber (left two photos). After the mixing of the two types of cells (middle) and application of the device, each type of cell in the collected (right upper) or flow-through (right lower) fraction was numerated. Arrow, cultured BMSCs; arrowhead, peripheral leukocytes. (**B**) Collection efficacy for human BMSCs (black box) and peripheral leukocytes (gray box). Each type of cell was applied to the device separately, and collection efficacy was calculated from the number of cells in the collected and flow-through fractions. (**C**) Collection efficacy for human BMSCs (black box) and peripheral leukocytes (gray box). Equal numbers of BMSCs and peripheral leukocytes were mixed and applied to the device. Collection efficacy was calculated from the number of cells in the collected and flow-through fractions. (**D**) Collection efficacy for CD44 (hatched box) and $CD45^+$ (dotted box) cells. Equal numbers of BMSCs and peripheral leukocytes were mixed and applied to the device. Cells positive for CD44 or CD45 in the collected or flow-through fraction were numerated by fluorescence-activated cell sorting (FACS), and collection efficacy was calculated from the number of positive cells in the cell mixture before the treatment. (**E**) Collection efficacy for mononuclear cells (MNCs) from canine bone marrow. $^{**}p < 0.01$ (**F**) Total number of CFUs derived from canine MNCs collected in the collected and flow-through fractions. From the results on collection efficacy and number of CFUs, the total number of CFUs was calculated. $^{**}p < 0.01$. (**G**) Collection efficacy for MNCs from human bone marrow. (**H**) Total number of CFUs derived from human MNCs collected in the collected and flow-through fractions. $^{**}p < 0.01$.

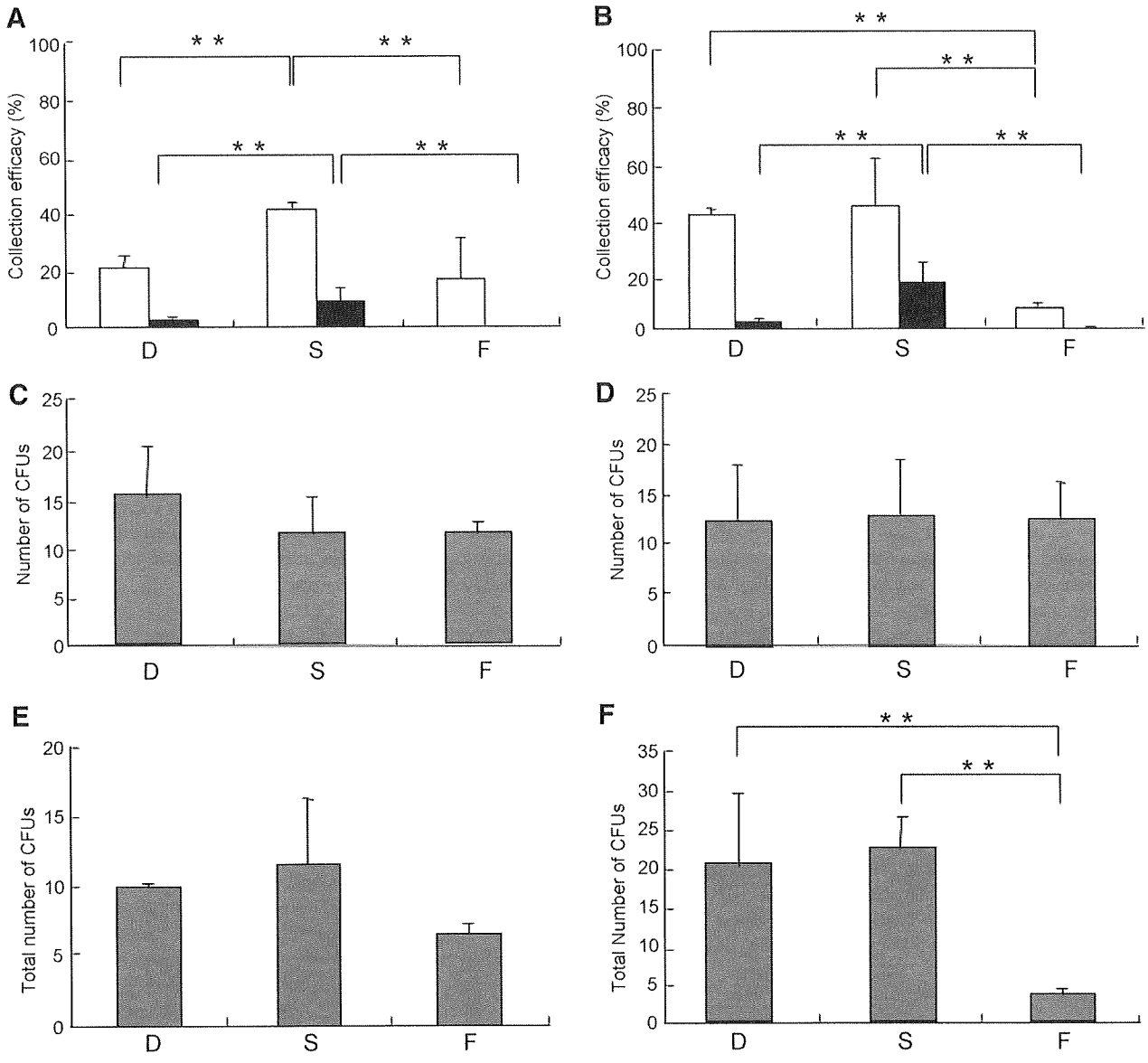

G

	Method of cell collection		
	D	S	F
Processing Time (min)	8.4±1.1**1,**2	18.8±2.9**1	56.5±3.4**2

FIG. 3. Device selectively prepares MNCs with CFUs. Collection efficacy for MNCs (white box) and erythrocytes (black box) isolated with each method from canine (**A**) and human (**B**) bone marrow. D, S, or F indicates each method described in Materials and Methods section. $^{**}p < 0.01$. Number of CFUs derived from equal numbers (2.5×10^5) of MNCs isolated by each method from canine (**C**) and human (**D**) bone marrow. Total number of CFUs derived from equal amounts of canine (**E**) and human (**F**) bone marrow using each method. $^{**}p < 0.01$. (**G**) Processing time for each method. $^{**1}p < 0.01$; $^{**2}p < 0.01$.

Selective collection of colony-forming cells from bone marrow by the device

Next, the selectivity of the device was analyzed using cells derived from canine (Fig. 2E, F) and human (Fig. 2G, H) bone marrow. In both cases, most erythrocytes passed through the filter and were collected in the flow-through fraction. Only a few were found in the collected fraction (data not shown). For canine bone marrow, the number of MNCs was significantly smaller in the collected fraction than in the

flow-through fraction ($p = 0.002$; Fig. 2E). The number of CFUs, however, was much higher in the collected fraction ($p < 0.001$; Fig. 2F). For human bone marrow, the number of MNCs in the collected and flow-through fraction did not differ (Fig. 2G). However, the number of CFUs was much higher in the collected fraction than in the flow-through fraction ($p < 0.001$; Fig. 2H). These results indicated the selective collection of CFUs by the device.

Comparison of method D with methods S and F

The biological properties of cells isolated by each of the three methods were compared. First, we compared the collection efficacy of method D with that of method S or F. ANOVA revealed significant differences among the collection efficacies for MNCs (canine, $p = 0.024$; human, $p = 0.0002$). Comparisons between individual methods were then carried out using Turkey's *post hoc* test. For canine bone marrow, the collection efficacy for MNCs was significantly lower with method D ($20.7 \pm 4.2\%$) than method S ($41.6 \pm 1.6\%$) ($p < 0.01$; Fig. 3A), and the same between method D and method F ($16.8 \pm 14.0\%$) (Fig. 3A). As for contamination by erythrocytes, method S showed larger numbers than method D or F. For human bone marrow, there was no difference in collection efficacy between method D ($40.5 \pm 14.5\%$) and method S ($43.9 \pm 10.8\%$) (Fig. 3B), and method F ($7.3 \pm 1.8\%$) was significantly less efficient than method D ($p < 0.01$; Fig. 3B). The number of contaminating RBCs was again high with method S (Fig. 3B). Next, the MNCs collected by each method were seeded on plastic dishes, and the number of CFUs was counted 14 days later. ANOVA indicated no significant difference among the numbers of CFUs of MNCs prepared by the three methods in canine ($p = 0.40$) and human bone marrow ($p = 0.95$) (Fig. 3C, D). From the results on collection efficacy and number of CFUs, the total number of CFUs isolated from bone marrow was calculated for each method. In the case of canine bone marrow, the total number of CFUs with method D (10.1 ± 0.2) was equivalent to that with method S (11.7 ± 4.7) and much larger than that with method F, but not significant (6.6 ± 0.1) (Fig. 3E). Similar results were obtained with human bone marrow cells. The total number of CFUs with method D (20.3 ± 9.4) was equivalent to that with method S (22.3 ± 4.4), and much larger than that with method F (3.6 ± 1.0) ($p < 0.01$; Fig. 3F). These results indicated that the device collected colony-forming cells from bone marrow with an efficacy equal to that of current methods requiring centrifugation. In addition, the processing time for method D (8.4 ± 1.1 min; Fig. 3G) was significantly shorter than that for the other methods (method S, 18.8 ± 2.9 min; method F, 56.5 ± 3.4 min) (ANOVA, $p < 0.001$; Turkey's *post hoc* test, $p < 0.01$; Fig. 3G).

Expression of MSC markers in isolated BMSCs

To compare the cell population isolated by each of the three methods, the expression of cell surface markers was analyzed by fluorescence-activated cell sorting (FACS). Because a combination of markers is more reliable, we focused on $CD10^+/CD271^+$, $CD90^+/CD271^+$, or $CD106^+/STRO\text{-}1^+$ double-positive cells. The $CD90^+/CD271^+$ and the $CD106^+/STRO\text{-}1^+$ populations were significantly larger among cells collected by method D than those collected by method S or method F (ANOVA, $p < 0.001$; Turkey's *post hoc* test, $p < 0.01$ for $CD90^+/CD271^+$, $p < 0.05$ for $CD106^+/STRO\text{-}1^+$, respectively; Fig. 4A, B).

Differentiation potential of isolated BMSCs

To analyze their potential to differentiate, the BMSCs isolated by each of the methods were propagated on culture

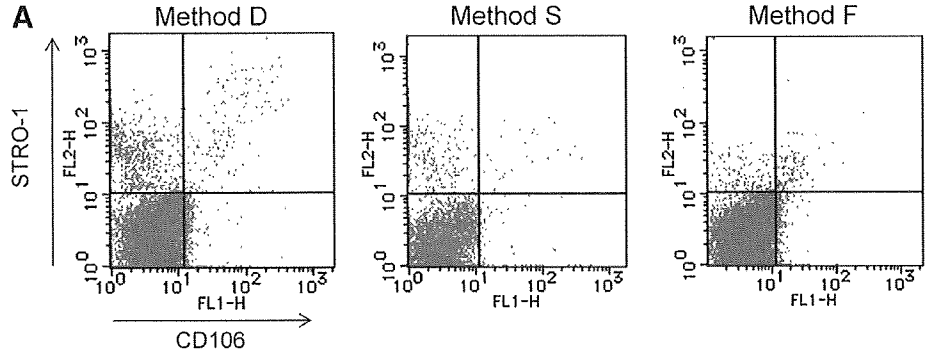

B

Markers	Fraction of double positive cells		
	Method D	Method S	Method F
$CD10^+$ / $CD271^+$	0.16 ± 0.05	0.13 ± 0.05	0.13 ± 0.02
$CD90^+$ / $CD271^+$	0.13 ± 0 **1**2	0.06 ± 0.01 **1*3	0.01 ± 0.01 *2*3
$CD90^+$ / $CD166^+$	0.31 ± 0.02	0.18 ± 0.12	0.23 ± 0.15
$CD106^+$ / $STRO\text{-}1^+$	1.61 ± 0.37 *1*2	0.48 ± 0.19 *1	0.71 ± 0.42 *2

FIG. 4. Device selectively prepares MNCs, which express mesenchymal marker. (**A**) FACS analysis of CD106 and STRO-1 on MNCs isolated by each method. (**B**) Fraction of cells double-positive for mesenchymal stem cell (MSC) markers among MNCs isolated by each method. **1,**2$p < 0.01$; *1,*2,*3$p < 0.05$.

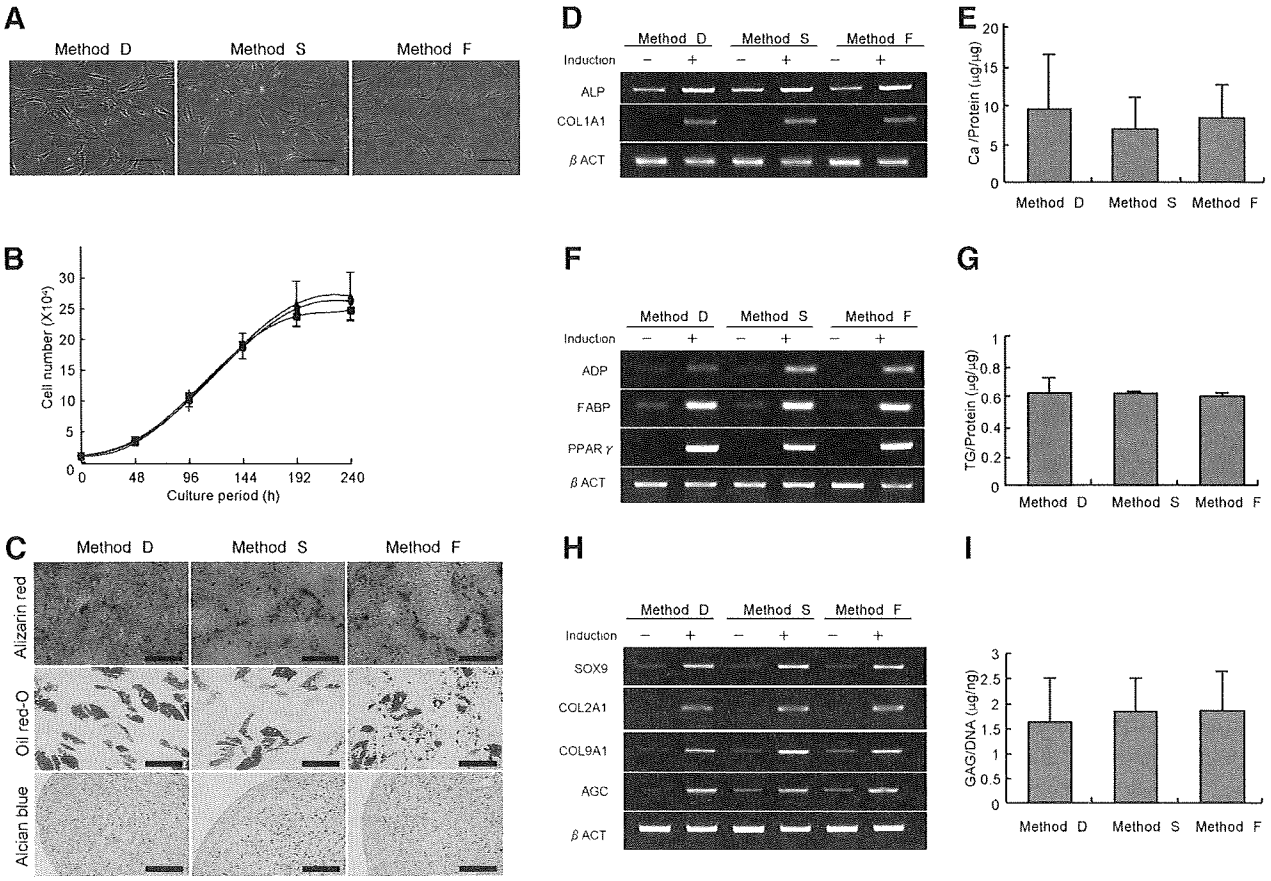

FIG. 5. Growth and differentiation potential of human BMSCs isolated by each method. The same numbers of BMSCs isolated by the three methods from human bone marrow were propagated on culture dishes for 2 weeks under standard conditions. (**A**) Microscopic views of cultured BMSCs isolated by each method. Magnification, 100×. Scale bars = 100 μm. (**B**) Growth of cultured BMSCs isolated by each method. ●, Method D; ▲, method S; ■, method F. (**C**) Differentiation potential of BMSCs isolated by each method. Osteogenic differentiation was analyzed by alizarin red staining. Magnification, 100×. Scale bars = 100 μm. Adipogenic differentiation was analyzed by oil red-O staining. Magnification, 100×. Scale bars = 100 μm. Chondrogenic differentiation was analyzed by alcian blue staining. Magnification, 40×. Scale bars = 300 μm. (**D**) Expression of bone-related genes before and after osteogenic induction. *ALP*, alkaline phosphatase. (**E**) Ca content after osteogenic induction. Ca, calcium. (**F**) Expression of fat-related genes before and after adipogenic induction. *ADP*, adipsin; *FABP*, fatty acid–binding protein; *PPARγ*, peroxisome proliferator-activated receptor gamma. (**G**) TG content after adipogenic induction. TG, triglyceride. (**H**) Expression of cartilage-related genes before and after chondrogenic induction. *AGC*, aggrecan. (**I**) GAG content after chondrogenic induction. GAG, glycosaminoglycan.

dishes and incubated for 2 weeks under standard growth conditions for MSCs. They were then induced to undergo osteogenesis, adipogenesis, and chondrogenesis. The morphology of the cells isolated by each of the methods was almost the same for both canine (Supplemental Fig. S2A, available online at www.liebertonline.com) and human (Fig. 5A) BMSCs. There was no difference in growth profile among the three methods in canine (Supplemental Fig. S2B, available online at www.liebertonline.com) or human (Fig. 5B) BMSCs. Osteogenic differentiation potential was evaluated with histochemical (alizarin red staining; Fig. 5C), mRNA expression (expression of the *ALP* and *COL1A1* genes; Fig. 5D), and biochemical (calcium content; Fig. 5E) analyses. There was no significant difference among the cells isolated by each of the three methods (ANOVA, $p = 0.61$). Similar results were observed in adipogenic differentiation

FIG. 6. Regeneration of bone tissues by cells isolated with the device. Data for six dogs at 4 weeks after the operation are presented. Frontal (**A**) and sagittal (**B**) views of micro-computed tomography. (**C**) Morphometrical analyses. The results of X-ray and micro-computed tomography were evaluated using the criteria described in the Materials and Methods section. Bone weight and volume were actually measured. $^{**}p < 0.01$; $^{*}p < 0.05$. CHR, carpal height ratio. (**D**) Histological analyses by hematoxylin–eosin staining. Magnification, 100×. Scale bar = 500 μm. (**E**) Fraction of regenerated bone tissue of each grade. Grade 1, white box; grade 2, gray box; grade 3, black box. $^{*}p < 0.05$. (**F**) Histological analyses using silver impregnation staining. Magnification, 200×. Scale bar = 200 μm. (**G**) Fraction of β-tricalcium phosphate with integrated collagen fibers of each grade. Grade 1, white box; grade 2, gray box; grade 3, black box. $^{*}p < 0.05$.

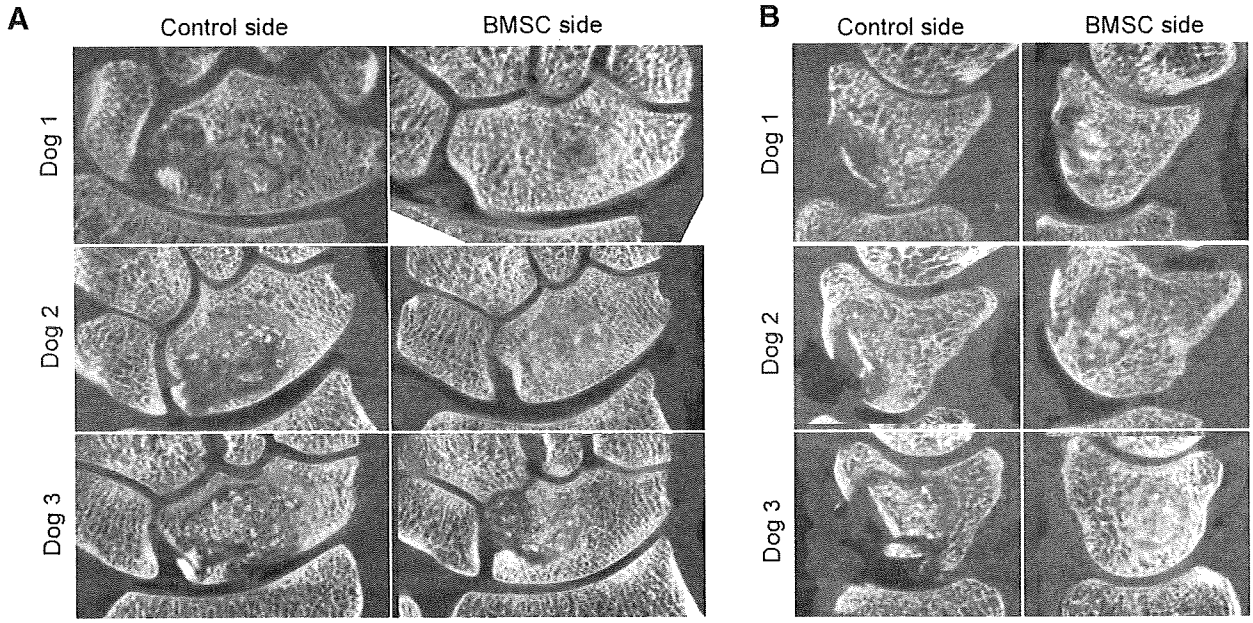

C

	X-ray evaluation		Micro CT evaluation			Actual Measurement		
	CHR	Ståhl index (%)	Bone Volume (cm^3)	Total Volume (cm^3)	Bone ratio	Weight (g)	Volume (cm^3)	Weight/Volume
Control side	0.30 ±0.03 * *	67.6 ±2.4 *	0.56 ±0.07 * *	0.81 ±0.11	0.67 ±0.03 * *	1.78 ±0.22 *	1.33 ±0.16 *	1.34 ±0.03 *
BMSC side	0.32 ±0.03 * *	72.1 ±6.3 *	0.64 ±0.06 * *	0.85 ±0.10	0.76 ±0.03 * *	1.83 ±0.19 *	1.34 ±0.15 *	1.38 ±0.04 *

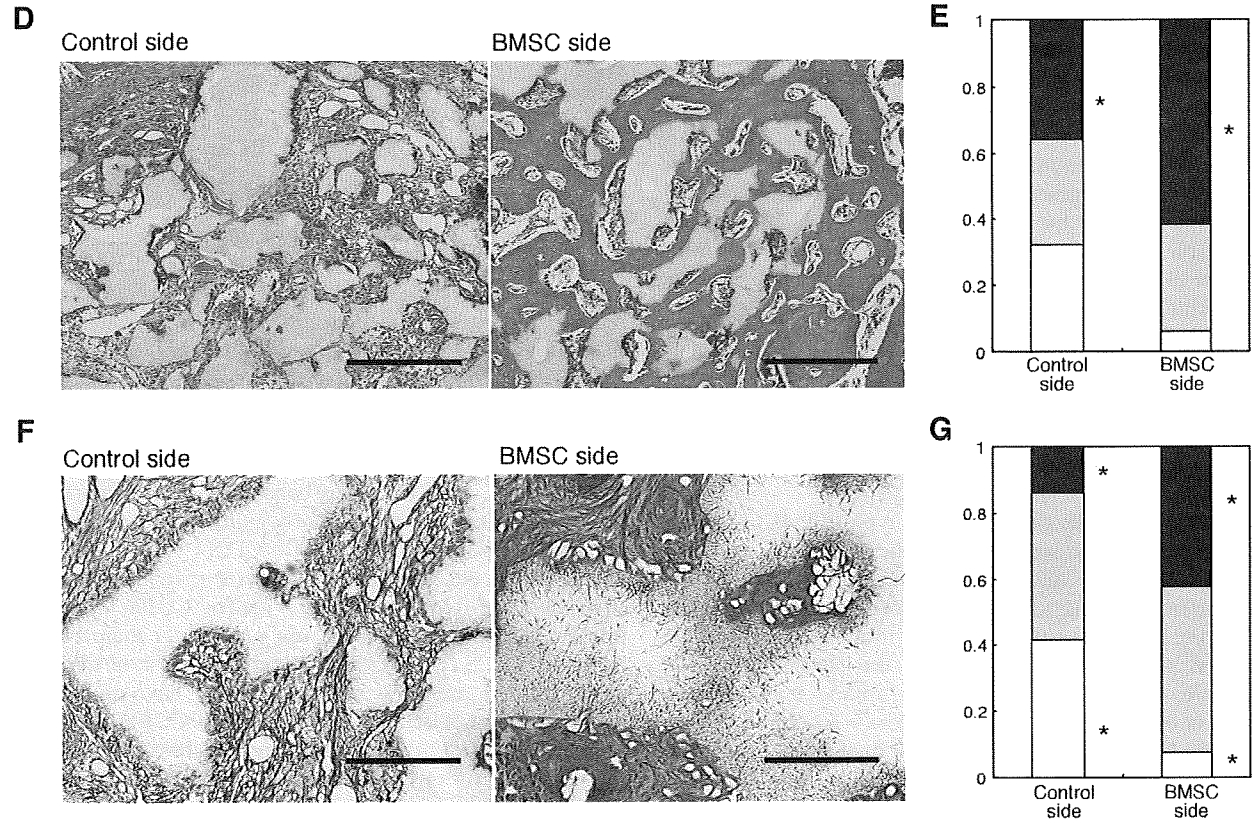

(ANOVA, $p = 0.41$; Fig. 5C, F, G) and chondrogenic differentiation (ANOVA, $p = 0.97$; Fig. 5C, H, I). Same results were obtained in the analyses of canine BMSCs (Supplemental Fig. S2C, available online at www.liebertonline.com). These results suggested that BMSCs isolated by each of the three methods had the multidirectional differentiation potential of MSCs.

Regeneration of bone tissues by cells isolated with the device

To confirm the *in vivo* osteogenic potential of cells collected with the device, we used the cells to regenerate bone tissues in a model of osteonecrosis using canine scapho-lunates, which we established previously.[15] Micro-CT findings at 4 weeks after the operation indicated bone regeneration to be more prominent on the BMSC side than control side in all cases (Fig. 6A, B). Carpal height ratio and the Ståhl index calculated from plain X-rays show the degree of collapse of scapholunate bone. Both parameters were significantly higher on the BMSC side than control side (Fig. 6C). Total volume and bone volume were analyzed from the micro-CT data. Bone volume and therefore bone ratio were greater on the BMSC side (Fig. 6C). Both actual weight and volume were also significantly higher on the BMSC side (Fig. 6C). These quantitative analyses suggested that the application of BMSCs prepared by the device contributed significantly to bone regeneration.

After the physical and radiological examinations, samples were processed for histological analyses. Microscopic findings of samples taken from the control side showed that a large amount of β-TCP remained unabsorbed, although multinucleated giant cells were found adjacent to β-TCP. In contrast, abundant new bone with the active absorption of β-TCP by multinucleated giant cells was found on the BMSC side (Fig. 6D). The extent to which β-TCP was absorbed as new bone formed was scored using criteria described in the Materials and Methods section. The grade 3 fraction was significantly larger on the BMSC side ($p = 0.032$; Fig. 6E).

To analyze the interaction between the prepared cells and β-TCP, silver impregnation staining was performed (Fig. 6F). The staining shows the invasion of collagen fibers into biodegradable materials. Collagen fibers in β-TCP granules adjacent to regenerated bone tissue were abundant on the BMSC side, but rare on the control side (Fig. 6F). Quantitative analyses showed the extent of the invasion to be significantly greater on the BMSC side ($p = 0.034$; Fig. 6G). These results suggested that BMSCs prepared using the device enhanced bone regeneration *in vivo*.

Discussion

Bone marrow cells consist of two types of MNCs: hematopoietic cells including hematopoietic stem cells, and stromal cells including MSCs. Approximately 99% of MNCs in bone marrow belong to the former population, and among the stromal cells, less than 5% have multidirectional differentiation potential compatible with the concept of MSCs. Therefore, the proportion of MSCs among bone marrow MNCs is estimated at less than 0.05%.[19] To obtain BMSCs including MSCs from bone marrow, it is essential to separate the hematopoietic MNCs.

Takenaka developed a novel filter composed of nonwoven fabrics to trap peripheral leukocytes for the treatment of autoimmune disease.[10] Because erythrocytes are deformed, which allows them to pass through small pores and have low adhesiveness, they can be separated from MNCs by the filter.[10] They used fibers 1.7 μm in diameter, because all the leukocytes were trapped when the fiber was less than 3 μm in diameter.[10] This filter, however, is not applicable to the separation of MSCs from hematopoietic MNCs, both of which will be captured, making it difficult to separate them by cell size. Therefore, we used fibers 15 μm in diameter with greater affinity for BMSCs than hematopoietic MNCs. MSCs are more adherent than hematopoietic cells.[4,19] MSCs adhere much more tightly to highly hydrophilic and rough surfaces than to hydrophobic and smooth surfaces.[20] The contact angle of the nonwoven fabric in the current device is estimated to be 20°, which is highly hydrophilic and may make it possible to trap MSCs in the device. This adherent trapping method may prevent excess shearing stress caused by the flow. Cells isolated by the device showed no increase in bradykinine or lactate dehydrogenase (LDH) (data not shown). In addition, mRNA expression of the *p16* and *p53* genes was not increased, and the karyotype showed no abnormalities (data not shown).

In terms of its potential clinical applications, the device has several advantages. The filter is composed of rayon and polyethylene. Rayon is used for the dialysis membranes of hemodialyzers and known to decrease platelet activity.[21] Polyethylene is a biomaterial employed in total hip replacement and as a scaffold for tissue engineering.[22] Therefore, all the materials are safe for clinical use. The isolation of BMSCs in a closed system is a major advantage of this device. Centrifugation requires mixing with an appropriate solution, which has to be performed in an open system. Current guidelines require the centrifugation process to be performed in an isolated area with specialized equipment. Because all steps can be done in a closed system, the device can isolate BMSCs from bone marrow on the operation table. Further, processing time is shorter than for the other two methods (Fig. 3G), which may help to reduce cell death during the isolation procedures. In addition, the method does not require special skills, which will help to obtain constant results and also be an advantage for clinical application.

We have shown that in terms of differentiation potential, the cells isolated using the device were equivalent to those prepared by current methods using centrifugation. The total number of CFUs obtained from bone marrow was equal to that achieved with method S and higher than that obtained with method F, suggesting that the device recovers almost all cells with the ability to form CFUs. FACS analyses showed that the method was superior to others in terms of the recovery of the MSC marker-positive population. CD10, CD44, CD90, CD106, and STRO-1 are considered surface markers of MSCs,[13,23] and, recently, CD271 was identified as a marker of MSCs.[24] The fractions of $CD90^+/CD271^+$ cells were larger among cells collected using the device than those isolated with the other two methods (Fig. 4). The $CD106^+/STRO\text{-}1^+$ fraction ($1.61 \pm 0.37\%$; Fig. 4) was even larger than that collected by FACS ($1.4 \pm 0.3\%$),[25] which has a risk of microbial contamination and unfavorable effects. We have no clear explanation for this selective collection. Because $CD106^+/STRO\text{-}1^+$ cells attach to plastic dish efficiently and have high colony-forming activity,[26] one possibility is that $CD106^+/STRO\text{-}1^+$ cells have high affinity to the filter materials used in the device. Finally, we have shown that the direct application of the trapped cells without *ex vivo* cultivation assisted the regeneration of bone

tissue *in vivo* (Fig. 6), although the role of transplanted cells may not be simply to reconstitute bone tissues by themselves but also to produce cytokines stimulating host cells,[15] suggesting that BMSCs collected with the new device on the operating table could be used for conditions requiring an acceleration of bone regeneration such as the nonunion of bone fractures.

Acknowledgments

We thank Dr. H. Iwata for suggestions and Drs. M. Neo, S. Fujibayashi, M. Takemoto, H. Ito, and H. Yoshitomi for clinical samples. This work was supported by Grants-in-aid for Scientific Research from the Japan Society for the Promotion of Science; from the Ministry of Education, Culture, Sports, Science, and Technology; from the Ministry of Health, Labor, and Welfare; and from the New Energy and Industrial Technology Development Organization.

Disclosure Statement

No competing financial interests exist.

References

1. Caplan, A.I. Mesenchymal stem cells. J Orthop Res **9,** 641, 1991.
2. Wagner, W., and Ho, A.D. Mesenchymal stem cell preparations comparing apples and oranges. Stem Cell Rev **3,** 239, 2007.
3. Peterson, E.A., and Evans, W.H. Separation of bone marrow cells by sedimentation at unit gravity. Nature **214,** 824, 1967.
4. Caterson, E.J., Nesti, L.J., Danielson, K.G., and Tuan, R.S. Human marrow-derived mesenchymal progenitor cells: isolation, culture expansion, and analysis of differentiation. Mol Biotechnol **20,** 245, 2002.
5. Li, Y., Ma, T., Yang, S.T., and Kniss, D.A. Thermal compression and characterization of three-dimensional nonwoven PET matrices as tissue engineering scaffolds. Biomaterials **22,** 609, 2001.
6. Takahashi, Y., and Tabata, Y. Effect of the fiber diameter and porosity of non-woven PET fabrics on the osteogenic differentiation of mesenchymal stem cells. J Biomater Sci Polym Ed **15,** 41, 2004.
7. Ma, Z., Kotaki, M., Yong, T., He, W., and Ramakrishna, S. Surface engineering of electrospun polyethylene terephthalate (PET) nanofibers towards development of a new material for blood vessel engineering. Biomaterials **26,** 2527, 2005.
8. Gador, W., and Jankowska, E. Filtration properties of nonwovens. Int J Occup Saf Ergon **5,** 361, 1999.
9. Gorman, N.E. Nonwoven materiel: manufacturing processes for sterilization wraps. Hosp Mater Manage Q **9,** 1, 1988.
10. Takenaka, Y. Lymphocytapheresis. Artif Organs **20,** 914, 1996.
11. Onodera, H., Abe, Y., Yoshida, M., Yamawaki, N., Yamashita, Y., Matsuo, H., Ichinose, K., Otsuru, I., and Shibuya, N. A new device for selective removal of $CD4^+$ T cells. Ther Apher **2,** 37, 1998.
12. Shibata, K.R., Aoyama, T., Shima, Y., Kenichi, F., Otsuka, S., Furu, M., Kohne, Y., Ito, K., Fujibayashi, S., Meo, M., Nakayama, T., Nakamura, T., and Toguchida, J. Expression of the p16INK4A gene is associated closely with senescence of human mesenchymal stem cells and is potentially silenced by DNA methylation during *in vitro* expansion. Stem Cells **25,** 2371, 2007.
13. Pittenger, M.F., Mackay, A.M., Beck, S.C., Jaiswal, R.K., Douglas, R., Mosca, J.D., Moorman, M.A., Simonetti, D.W., Craig, S., and Marshak, D.R. Multilineage potential of adult human mesenchymal stem cells. Science **284,** 143, 1999.
14. Fukiage, K., Aoyama, T., Shibata, K.R., Otsuka, S., Furu, M., Kohno, Y., Ito, K., Jin, Y., Fujita, S., Fujibayashi, S., Neo, M., Nakayama, T., Nakamura, T., and Toguchida, J. Expression of vascular cell adhesion molecule-1 indicates the differentiation potential of human bone marrow stromal cells. Biochem Biophys Res Commun **365,** 406, 2008.
15. Ikeguchi, R., Kakinoki, R., Aoyama, T., Shibata, K.R., Otsuka, S., Fukiage, K., Nishijo, K., Ishibe, T., Shima, Y., Otsuki, B., Azuma, T., Tsutsumi, S., Nakayama, T., Otsuka, T., Nakamura, T., and Toguchida, J. Regeneration of osteonecrosis of canine scapholunate using bone marrow stromal cells: possible therapeutic approach for Kienböck disease. Cell Transplant **15,** 411, 2006.
16. Youm, Y., McMurthy, R.Y., Flatt, A.E., and Gillespie, T.E. Kinematics of the wrist. I. An experimental study of radial-ulnar deviation and flexion-extension. J Bone Joint Surg Am **60,** 423, 1978.
17. Goldfarb, C.A., Hsu, J., Gelberman, R.H., and Boyer, M.I. The Lichtman classification for Kienböck's disease: an assessment of reliability. J Hand Surg Am **28,** 74, 2003.
18. Ogose, A., Kondo, N., Umezu, H., Hotta, T., Kawashima, H., Tokunaga, K., Ito, T., Kudo, N., Hoshino, M., Gu, W., and Endo, N. Histological assessment in grafts of highly purified beta-tricalcium phosphate (OSferion) in human bones. Biomaterials **27,** 1542, 2006.
19. Chamberiain, G., Fox, J., Ashton, B., and Middleton, J. Concise review: mesenchymal stem cells: their phenotype, differentiation capacity, immunological features, and potential for homing. Stem Cells **25,** 2739, 2007.
20. Kim, M.S., Shin, Y.N., Cho, M.H., Kim, S.H., Kim, S.K., Cho, Y.H., Khang, G., Lee, I.W., and Lee, H.B. Adhesion behavior of human bone marrow stromal cells on differentially wettable polymer surfaces. Tissue Eng **13,** 2095, 2007.
21. Thijs, A., Grooteman, M.P., Zweegman, S., Nubé, M.J., Huijgens, P.C., and Stehouwer, C.D. Platelet activation during haemodialysis: comparison of cuprammonium rayon and polysulfone membranes. Blood Purif **25,** 389, 2007.
22. Tessmar, J.K., and Göpferich, A.M. Customized PEG-derived copolymers for tissue-engineering applications. Macromol Biosci **7,** 23, 2007.
23. Deans, R.J., and Moseley, A.B. Mesenchymal stem cells: biology and potential clinical uses. Exp Hematol **28,** 875, 2000.
24. Bühring, H.J., Battula, V.L., Treml, S., Schewe, B., Kanz, L., and Vogel, W. Novel markers for the prospective isolation of human MSC. Ann NY Acad Sci **1106,** 262, 2007.
25. Gronthos, S., and Zannettino, A.C. A method to isolate and purify human bone marrow stromal stem cells. Methods Mol Biol **449,** 45, 2008.
26. Gronthos, S., Zannettino, A.C., Hay, S.J., Shi, S., Graves, S.E., Kortesidis, A., and Simmons, P.J. Molecular and cellular characterisation of highly purified stromal stem cells derived from human bone marrow. J Cell Sci **116,** 1827, 2003.

Address correspondence to:
Tomoki Aoyama, M.D., Ph.D.
Institute for Frontier Medical Sciences
Kyoto University
53 Kawahara-cho
Shogoin, Sakyo-ku
Kyoto 606-8507
Japan

E-mail: blue@frontier.kyoto-u.ac.jp

Received: December 21, 2008
Accepted: April 13, 2009
Online Publication Date: July 6, 2009

Journal of Neuroscience Research 87:576–585 (2009)

Nicotinic Receptor Stimulation Protects Nigral Dopaminergic Neurons in Rotenone-induced Parkinson's Disease Models

Hiroki Takeuchi,[1] Takashi Yanagida,[2] Masatoshi Inden,[2] Kazuyuki Takata,[2] Yoshihisa Kitamura,[2] Kentaro Yamakawa,[3] Hideyuki Sawada,[3] Yasuhiko Izumi,[4] Noriyuki Yamamoto,[4] Takeshi Kihara,[4] Kengo Uemura,[1] Haruhisa Inoue,[1] Takashi Taniguchi,[2] Akinori Akaike,[4] Ryosuke Takahashi,[1] and Shun Shimohama[5]*

[1]Department of Neurology, Graduate School of Medicine, Kyoto University, Kyoto, Japan
[2]Department of Neurobiology, Kyoto Pharmaceutical University, Kyoto, Japan
[3]Clinical Research Center, National Hospital Organization Utano National Hospital, Kyoto, Japan
[4]Department of Pharmacology, Graduate School of Pharmaceutical Sciences, Kyoto University, Kyoto, Japan
[5]Department of Neurology, Sapporo Medical University, Sapporo, Japan

Parkinson's disease (PD) is the second most common neurodegenerative disease and is characterized by dopaminergic (DA) neuronal cell loss in the substantia nigra. Although the entire pathogenesis of PD is still unclear, both environmental and genetic factors contribute to neurodegeneration. Epidemiologic studies show that prevalence of PD is lower in smokers than in nonsmokers,. Nicotine, a releaser of dopamine from DA neurons, is one of the candidates of antiparkinson agents in tobacco. To assess the protective effect of nicotine against rotenone-induced DA neuronal cell toxicity, we examined the neuroprotective effects of nicotine in rotenone-induced PD models in vivo and in vitro. We observed that simultaneous subcutaneous administration of nicotine inhibited both motor deficits and DA neuronal cell loss in the substantia nigra of rotenone-treated mice. Next, we analyzed the molecular mechanisms of DA neuroprotective effect of nicotine against rotenone-induced toxicity with primary DA neuronal culture. We found that DA neuroprotective effects of nicotine were inhibited by dihydro-β-erythroidine (DHβE), α-bungarotoxin (αBuTx), and/or PI3K-Akt/PKB (protein serine/threonine kinase B) inhibitors, demonstrating that rotenone-toxicity on DA neurons are inhibited via activation of α4β2 or α7 nAChRs-PI3K-Akt/PKB pathway or pathways. These results suggest that the rotenone mouse model may be useful for assessing candidate antiparkinson agents, and that nAChR (nicotinic acetylcholine receptor) stimulation can protect DA neurons against degeneration.

Key words: Parkinson's disease; rotenone; nicotine; dopaminergic neuron; neuroprotection

Parkinson's disease (PD) is the second most common progressive neurodegenerative disorder. It is characterized by relatively selective degeneration of dopaminergic neurons in the substantia nigra and loss of dopamine in the striatum resulting in resting tremor, rigidity, bradykinesia and postural instability (Dunnett and Björklund, 1999; Shimohama et al., 2003). Although the pathogenesis of PD is still unclear, it is thought that both environmental and genetic factors cause neurodegeneration. Rural residency, pesticides and intrinsic toxic agents were reported as environmental risk factors for sporadic PD. Recent studies revealed several mutations in familial PD genes such as α-synuclein, parkin, PINK1, LRRK2 (leucine-rich repeat kinase 2), DJ-1, and UCH-L1 (ubiquitin C-terminal hydrolase-L1) (Schapira, 2006). Epidemiological studies suggest that the use of pesticides increases the risk of PD, possibly via reduced activity of complex I in the mitochondrial respiratory chain in the substantia nigra and result in the pathogenesis of PD (Parker et al., 1989; Mann et al., 1992; Mizuno et al., 1998). 6-hydroxydopamine (6-OHDA), a H_2O_2 pro-oxidant and 1-methyl-4-phenyl-1,2,3,6-tetrahydropyridine (MPTP), a mitochondrial complex I inhibitor, have been widely used to produce toxin models of sporadic PD. Chronic exposure to rotenone, a nature-derived pesticide, could be a more

*Correspondence to: Shun Shimohama, MD, PhD, Department of Neurology, Sapporo Medical University, S1W17, Chuo-ku, Sapporo, 060-8556, Japan. E-mail: shimoha@sapmed.ac.jp

Received 18 March 2008; Revised 28 May 2008; Accepted 13 July 2008

Published online 19 September 2008 in Wiley InterScience (www.interscience.wiley.com). DOI: 10.1002/jnr.21869

appropriate animal PD model because rotenone-treated animals show slowly progressive DA neuronal loss, and Lewy body–like particles, which are primarily aggregations of α-synuclein (Betarbet et al., 2000, Inden et al., 2007).

On the other hand, current drug therapy is limited to supplementing dopamine (DA) or enhancing dopaminergic effect. Some may have neuroprotective effects, but their effects remain controversial (Quik, 2004; Du et al., 2005; Iravani et al., 2006). It has also been reported that smokers have a lower risk for PD (De Reuck et al., 2005; Wirdefeldt et al., 2005), and nAChRs (nicotinic acetylcholine receptor) were decreased in the brains of PD patients (Fujita et al., 2006) and PD model animals (Quik et al., 2006). Nicotine may up-regulate DA release at striatum from nigral dopaminergic neurons (Morens et al., 1995), followed by stimulation of α4β2 nAChRs (Champtiaux et al., 2003). Furthermore, nicotine could protect mitochondria and had protective effect from oxidative stress (Cormier et al., 2003; Xie et al., 2005). In studies made in vivo, stimulation of nAChRs resulted in neuroprotection in cerebral ischemia and PD model animals (Shimohama et al., 1998; Kagitani et al., 2000; Parain et al., 2003). In vitro, we have demonstrated that nicotine protected rat cortical neurons against glutamate toxicity and lower motor neurons against β-amyloid toxicity respectively, and that nicotine was antiapoptotic (Akaike et al., 1994; Kihara et al., 1997, 2001; Nakamizo et al., 2005). Also nicotine protected rat nigral dopaminergic neurons against 1-methyl-4-phenylpyridinium (MPP^+) cytotoxicity by non-α7 nAChR stimulation (Jeyarasasingam et al., 2002). So nicotinic receptor stimulation may be a good target for DA neuroprotective therapy toward PD. However, the further protective mechanisms for dopaminergic neurons have not been elucidated.

In this study, we investigated the neuroprotective effect of nicotine against nigral DA neuronal death induced by rotenone with a chronic rotenone-treated PD mouse model, and analyzed molecular mechanisms of the protection in dissociated cultures of the fetal rat ventral mesencephalon.

MATERIALS AND METHODS

Materials

Rotenone, (−)-nicotine hydrogen bitartrate, mecamylamine (Mec), αBuTx, DHβE, and triciribine, an Akt/PKB inhibitor, were purchased from Sigma (St. Louis, MO). LY294002, a PI3K (phosphatidylinositol 3-kinase) inhibitor was from Calbiochem (Darmstadt, Germany). Carboxylmethyl cellulose (CMC) was obtained from Nacalai Tesque (Kyoto, Japan). Mouse monoclonal antibodies against microtubule-associated protein 2 (MAP2), tyrosine hydroxylase (TH) and β-actin were purchased from Sigma. Rabbit polyclonal antibody against TH was from Chemicon (Temecula, CA).

Mouse Model and Drug Administration

Eight-week-old male C57BL/6J mice (20–25 g) were purchased from Japan SLC Inc. (Hamamatsu, Japan). The animals were acclimated and maintained at 23°C under a 12-hr light/dark cycle (lights on 09.00–21.00 hr). Mice were housed in standard laboratory cages and had free access to food and water throughout the study period. All animal experiments were carried out in accordance with the National Institutes of Health (NIH) Guide for the Care and Use of Laboratory Animals, and the protocols were approved by the Committee for Animal Research at Kyoto University. Rotenone was administrated orally once daily by gavage with a catheter at a dose of 30 mg/kg for 28 days. Rotenone was suspended in 0.5% CMC and administrated orally once daily at a concentration of 12 mL/kg body weight. The 0.5% CMC was administrated orally as vehicle to control mice (Inden et al., 2007). For in vivo experiments, nicotine ((−)-nicotine hydrogen bitartrate dissolved in saline) at a dose of 0.21 or 0.42 mg/kg (free base) was daily injected subcutaneously at 30 min before each oral administration of rotenone. Saline was injected in parallel as the corresponding vehicle control. Each group contained 6–12 mice.

Behavior Analysis

The behavior of each mouse was assessed by the rotarod treadmill test. The rotarod treadmill (accelerating model 7750, Ugo Basile, Varese, Italy) consists of a plastic rod, 6 cm in diameter and 36 cm long, with a nonslippery surface 20 cm above the base (trip plate). This rod is divided into four equal sections by five discs (25 cm in diameter), which enables four mice to walk on the rod at the same time. In the present study, the accelerating rotor mode was used (10-grade speeds from 3.5 to 35 r.p.m. for 5 min). Time was recorded while mice were running on the rod (from when they were put on the rod to when they fell off).

Immunohistochemistry

Mice were perfused with 10 mM phosphate-buffered saline (PBS) and then 4% paraformaldehyde in 100 mM phosphate buffer (PB) under deep anesthesia with pentobarbital (100 mg/kg, intraperitoneal injection). After perfusion, the brain was quickly removed and postfixed for 2 days and then transferred to 15% sucrose solution in 100 mM PB at 4°C at least for 4 days. After cryoprotection, the brain was rapidly frozen by heat exchange from vaporized CO_2 gas (−70°C) and then sections (60 μm) were cut with a cryostat and collected in 100 mM PBS containing 0.3% Triton X-100 (PBS-T). After several washes, the sections were stored until use in a free-floating state at 4°C for immunohistochemical analysis.

Brain sections were incubated with primary rabbit polyclonal antibody to TH (1:10,000), for 3 days at 4°C, and next with biotinylated antibody to rabbit IgG (1:2000) for 2 hr at room temperature. Then the sections were incubated with avidin peroxidase (1:4000) with the ABC kit for 1 hr at room temperature. All sections were rinsed several times with PBS-T between incubations. Labeling was revealed by DAB (3-3′-diaminobenzidine tetrahydrochloride) with nickel ammonium, which yielded a dark blue color.

Stereological Analysis

The total number of dopaminergic neurons in both hemispheres of the substantia nigra pars compacta (SNC) was

estimated by means of a fractionator-sampling design (Gundersen et al., 1988; West et al., 1991) and a former report (Baquet et al., 2005). Briefly, staining with the anti-TH antibody delineated the mediodorsal boundary of the SNC in each 60 μm cryostat section. We used every third coronal section to perform an analysis starting with the first appearance of TH-positive neurons and extending to the most caudal parts of the SNC and including both hemispheres. Cell counts were made at automatically determined intervals by the StereoInvestigator, a morphometry and stereology software package (version 5.0; MicroBrightField, Colchester, VT), within an unbiased counting frame of known area (100 × 100 μm^2) superimposed on the image. Sections were viewed under 40× magnification on an Olympus (Tokyo, Japan) BA51 photomicroscope, the StereoInvestigator, thereby creating a systematic random sample of the area, randomly positioned the counting frame within the SNC. We defined 16 μm as the z-dimension of the counting brick with a 2-μm guard on each side. Stained cells were counted within the outlines defined by TH expression, and total estimates were obtained.

Immunoblotting

After repeated rotenone administration for 28 days, the striatum (mixture of both right and left tissues) in treated mice were rapidly removed and homogenized with eight volumes of 50 mM Tris-buffered saline (pH 7.4) containing protease inhibitor cocktail (Roche Diagnostics, Mannheim, Germany). After centrifugation at 50,000*g* for 30 min, the supernatant was used as cytosolic fraction. Aliquots of cytosolic fractions containing 10 μg of protein were subjected to sodium dodecyl sulfate-polyacrylamide gel electrophoresis (SDS-PAGE) and then immunoblotted with mouse monoclonal antibody against TH (1:5000) and reblotted with anti–β-actin antibody (1:10,000). For semiquantitative analysis, bands of TH on radiographic films were scanned with a CCD color scanner (ARCUS II, AGFA, Leverkusen, Germany). Densitometric analysis was performed by the public domain program NIH Image 1.56 (by Wayne Rasband at the U.S. National Institutes of Health).

Primary Neuronal Cultures of the Ventral Mesencephalon

Cultures of rat mesencephalic cells were established according to methods described previously (Sawada et al., 2004). Briefly, the ventral two-thirds of the mesencephalon were dissected from rat embryos on the 16th day of gestation. The dissected regions included dopaminergic neurons from the substantia nigra and the ventral tegmental area but not noradrenergic neurons from the locus ceruleus. Neurons were dissociated mechanically and plated out onto 0.1% polyethylenimine-coated plastic coverslips at a density of 1.3 × 10^5 cells/cm^2. The culture medium consisted of Eagle's minimum essential medium containing 10% fetal calf serum for the first 1–4 days in culture and horse serum from the 5th day onward. Cultures were maintained at 37°C in a humidified atmosphere of 5% CO_2. Only mature cultures (8 days in vitro) were used for experiments. The animals were treated in accordance with guidelines published in the NIH Guide for the Care and Use of Laboratory Animals.

Treatment of Cultures

All experiments were carried out in Eagle's minimum essential medium with 10% horse serum at 37°C. First of all, cultured neurons were exposed to rotenone for 48 hr, except for pretreatment of LY294002 for 10 min to cause PI3K inhibition. After that, to show the time course, cultured neurons were administrated rotenone and/or nicotine for 12, 24, and 48 hr. Nicotine and nAChR antagonists (Mec, αBuTx, DHβE) were added to the medium simultaneously with rotenone. The concentration of each antagonist was the maximal dosage that did not show cytotoxicity or interference among nAChRs. Ki values of αBuTx were 2.16 (1.56–3.01) nM for α7 nAChR and >10,000 nM for α4β2nAChR, and those of DHβE were 7700 (4510–13,100) nM for α7 nAChR and 24.6 (16.9–35.8) nM for α4β2 nAChR (Grinevich et al., 2005). To confirm PI3K inhibition, LY294002 was administrated 10 min before the additional treatment of rotenone and nicotine. Triciribine was used simultaneously with rotenone and nicotine to inhibit Akt/PKB.

Immunocytochemistry and Evaluation of Neurotoxicity in Neuronal Cultures

Immunostaining was used to evaluate the number of dopaminergic neurons. Cultured cells were incubated with polyclonal rabbit anti-TH antibody (1:400) overnight at 4°C, then with biotinylated secondary antibody (1:200), and conjugated to avidin peroxidase (1:200) by the ABC kit (Vector Laboratories, Burlingame, CA) at room temperature for 1 hr. After that, they were labeled with a DAB staining kit (Nacalai, Kyoto, Japan). Neurotoxicity in each experiment was defined as a reduction in the survival rate, which was expressed as percentage survival relative to the survival observed in control cultures. For primary cultures, at least 200 dopaminergic neurons were counted in 30 randomly selected fields at 100× (total magnification) in control cultures to determine the total number of neurons. The total number of neurons was assessed by the method, described above, but using the anti-MAP2 antibody.

RNA Preparation From Rat Mesencephalic Cells

Total cell RNA was extracted with the Isogen RNA Isolation Kit (Nippon Gene, Japan) as originally described elsewhere (Chomczynski and Sacchi, 1987). The concentration of the isolated total RNA was determined spectrophotometrically at 260 nm. The first strand cDNA was synthesized with a reverse transcriptase–polymerase chain reaction (RT-PCR) kit purchased from GE Healthcare Bioscience (Giles, UK). Briefly, reverse transcription (RT) was carried out in a 15-μL reaction mixture containing 5 μg total RNA, 5 μL Bulk first-strand reaction mix, 1 μL DTT solution, and 1 μL $pd(N)_6$ primer, by incubation at 42°C for 20 min followed by denaturation at 99°C for 5 min and then quick-chilled on ice. The second strand cDNA synthesis/PCR amplification was performed in a mixture of 2 μL RT product, 2.5 μL 10× PCR buffer, 200 nM dNTP, 1.5 mM $MgCl_2$, 0.05 U/μL Ex

TABLE I. Paired Primers Used for RT-PCR Detection of nAChR Subunits*

Subunit	Primer	Nucleotide sequence	Size (bp)	Tm (°C)
α4	Forward	CTGGGTGCGTAGAGTCTTCC	239	62
	Reverse	TAGGCTGGGTCTCGACTGCT		
α7	Forward	TTTCTGCGCATGAAGAGGCCCGGAGAT	295	60
	Reverse	ACCTCCTCCAGGATCTT		
β2	Forward	AAGGTGGTCTTCCTGGAGAAGC	287	60
	Reverse	GCGTACGCCATCCACTGCT		
GAPDH	Forward	CGTCTTCACCACCATGGAGA	300	60
	Reverse	CGGCCATCACGCCACAGCTT		

*Tm, annealing temperature; Forward, sense primer; Reverse, antisense primer. GAPDH (glyceraldehyde-3-phosphate dehydrogenase) was used as the internal control for RNA detection.

Taq DNA polymerase, and 500 nM sense and antisense primers (Table I). The amplification protocol was as follows: initial denaturation at 94°C for 5 min; 30 cycles at 94°C for 30 sec, annealing at the respective temperature (Table I) for 30 sec, and 72°C for 1.5 min; a final extension at 72°C for 7 min with a GeneAmp 9700 thermal cycler (Perkin Elmer, Applied Biosystem, Forster City, CA). PCR products were electrophoresed on 2% agarose gels and stained with ethidium bromide (0.5 mg/mL). Then, the PCR products were visualized with an ultraviolet transilluminator coupled to a CCD camera.

Statistical Evaluation

Data was expressed as the ratio of surviving dopaminergic neurons relative to the number of neurons in vehicle-treated or in control group. Also, the density of TH by immunoblotting was assessed in the same manner. They are represented as the mean ± SEM. Statistical significance was determined by analysis of variance (ANOVA) followed by Bonferroni's multiple comparison test.

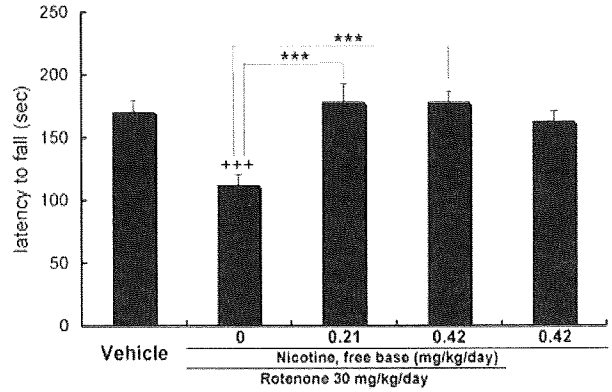

Fig. 1. Behavior analysis by rotarod treadmill test of chronically rotenone-treated mice. Nicotine administration improved impaired behavior induced by rotenone. One-way ANOVA was used for statistical analysis, followed by Bonferroni's multiple comparison test. Each value is the mean ± SEM, $n = 8$–12, $^{***}P < 0.001$, $^{+++}P < 0.001$ vs. vehicle.

RESULTS

Nicotine Treatment Improved Behavior Impaired by Rotenone

In our in vivo studies, we first checked the motor behavior of rotenone-treated model mice because it was important that the animals showed a close PD phenotype. The simultaneous daily administration of oral rotenone and subcutaneous nicotine prevented the motor impairment elicited by rotenone (Fig. 1). Nicotine alone showed no significant difference compared with the vehicle group. This animal model could be useful for assessing the bradykinesia/akinesia, one of the symptoms of PD.

Nicotine Treatment Improved Histological Findings in the Substantia Nigra

In the substantia nigra, oral treatment of rotenone decreased the number of dopaminergic neurons. On the other hand, the simultaneous daily administration of oral rotenone and subcutaneous nicotine prevented the decrease (Fig. 2A). Stereological assessment of the number of TH-positive cells in the bilateral SNC confirmed the histological findings with the statistical significance (Fig. 2B). That is, simultaneous administration of nicotine significantly protected dopaminergic cells in the midbrain of rotenone-treated mice from rotenone-induced neurotoxicity.

Nicotine Attenuated Rotenone-induced Axonal/Nerve Terminal Damage in the Striatum

The striatum was immunostained with the same antibody as the substantia nigra. About histological findings, the density of TH-positive neurons in the striatum of rotenone-treated mice seemed to be diminished compared with the vehicle group. Rotenone and nicotine treatment seemed to prevent the density from being decreased (Fig. 3A). Densitometric analysis of immunoblotting performed using the striatal lysate of each group showed that nicotine treatment remarkably improved the expression of TH from rotenone toxicity (Fig. 3B). In other words, these results confirmed that nicotine protected nigrostriatal dopaminergic neurons from the cell death by rotenone toxicity. α-Synuclein-positive aggregations were detected in the cell bodies of dopaminergic neurons of rotenone-treated mice, but the number was

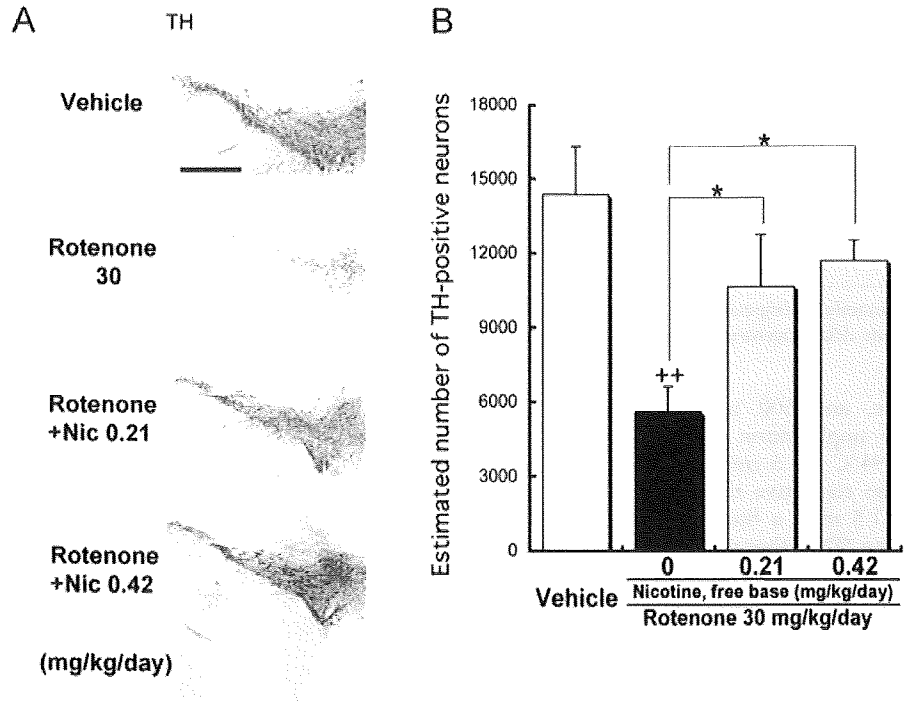

Fig. 2. Immunohistological analysis of nigral dopamine neurons. Nicotine improved the viability of dopaminergic cells against rotenone toxicity. Nic, Nicotine. **A:** Representative findings of each group. Scale bar = 500 μm. **B:** Stereological analysis of the number of the TH-positive neurons in the substantia nigra. One-way ANOVA was used for statistical analysis, followed by Bonferroni's multiple comparison test. Each value is the mean ± SEM, $n = 4$, $^{\star}P < 0.05$, $^{++}P < 0.01$ vs. vehicle.

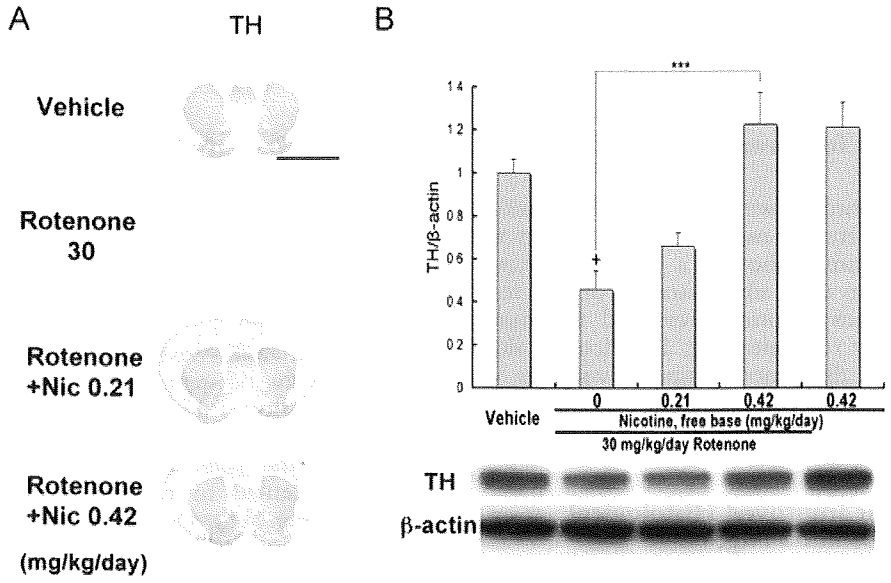

Fig. 3. Immunological analysis of striatal dopamine neurons. Nicotine improved the viability of dopaminergic cells against rotenone toxicity. **A:** Representative immunohistological findings of each group. Nic, Nicotine. Scale bar = 4 mm. **B:** Densitometric analysis of TH in striatal lysate. TH density was expressed as TH/β-actin ratio and relative density standardized by the results of vehicle group. One-way ANOVA was used for statistical analysis, followed by Bonferroni's multiple comparison test. Each value is the mean ± SEM, $n = 4$, $^{***}P < 0.001$, $^{+}P < 0.05$ vs. vehicle.

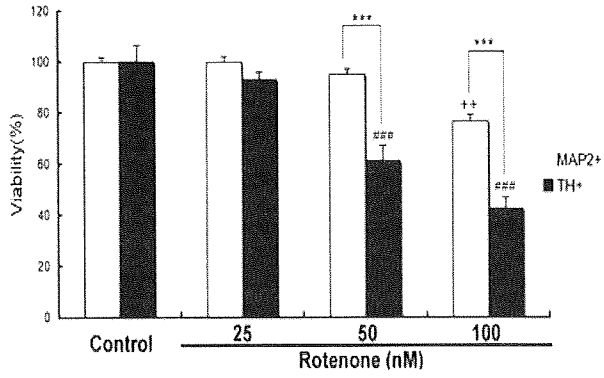

Fig. 4. Statistical analysis of rotenone-induced neuronal cell death in cultures of rat mesencephalic cells (day 8), standardized by the number of sham operations. It was suggested that dopaminergic neuron was more vulnerable against rotenone toxicity than other types of neurons. MAP2, microtubule-associated protein 2, a marker of central nervous system neurons; TH, tyrosine hydroxylase, a marker of dopaminergic neurons. Two-way factorial ANOVA was used for statistical analysis, followed by Bonferroni's multiple comparison test. Each value is the mean ± SEM, $n = 8$, $^{***}P < 0.001$, $^{++}P < 0.01$ vs. control (MAP2 positive), $^{###}P < 0.001$ vs. control (TH positive).

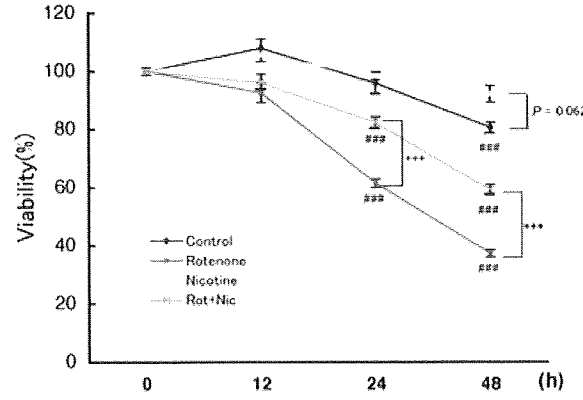

Fig. 5. Time course analysis of rotenone toxicity and nicotinic neuroprotection for TH-positive neurons, standardized by the number of control 0 hr. Both effects were shown after 24 hr since compounds were administrated. Rotenone, rotenone 100 nM; Nicotine, nicotine 100 μM; Rot+Nic, simultaneous administration of rotenone 100 nM and nicotine 100 μM. Two-way factorial ANOVA was used for statistical analysis, followed by Bonferroni's multiple comparison test. Each value is the mean ± SEM, $n = 8$, $^{###}P < 0.001$ vs. control 0 hr, $^{+++}P < 0.001$ vs. rotenone 24 hr, $^{***}P < 0.001$ vs. rotenone 48 hr.

too small to perform statistical assessment (data not shown).

Neuroprotective Effect of Nicotine Against Rotenone-induced Neurotoxicity in Cultures of Mesencephalic Neurons

Forty-eight-hour exposure to rotenone caused dose-dependent neurotoxicity, more remarkable in TH-positive neurons than in MAP2-positive cells, which represented the total neuronal cells (Fig. 4). This result showed that dopaminergic neurons were more vulnerable to rotenone-induced neurotoxicity. Time course experiment revealed that both rotenone toxicity and nicotinic neuroprotection were shown remarkably after 24 hr (Fig. 5). Immunostaining of TH showed that the viability of TH-positive cells was decreased by rotenone treatment and improved by addition of nicotine. Treatment with nicotine alone did not remarkably change the viability of TH-positive cells statistically (Fig. 5, Fig. 6A–D). Simultaneous administration of nicotine resulted in a dose-dependent increase of the viability of TH-positive cells (Fig. 6E). So nicotine treatment protected dopaminergic neurons against rotenone-induced neuronal death in a dose-dependent manner. This neuroprotective effect was inhibited by 100 μM Mec, a broad-spectrum nAChR antagonist (Fig. 7A), 100 nM αBuTx, an α7 nAChR antagonist (Fig. 7B), and 1 μM DHβE, an α4β2 antagonist (Fig. 7C). Treatment with the same concentrations of these antagonists or nicotine alone did not affect neurotoxicity. Nicotine-induced neuroprotection was therefore shown to occur via nAChRs, at least through α7 and α4β2 receptors. Also, RT-PCR (Fig. 7D) showed that mRNA of nAChRs subunits was expressed in rat mesencephalic cells. These results are relevant to the previous report that α7 and α4β2 nAChRs had biological activity in dopaminergic neurons in the midbrain (Champtiaux et al., 2003).

Nicotine-induced PI3K-Akt/PKB Pathway-activated Survival Activity of Dopaminergic Neurons

LY294002, a PI3K inhibitor inhibited nicotinic neuroprotection (Fig. 8A). Also triciribine, an Akt/PKB inhibitor, had the same effect (Fig. 8B). It is therefore likely that nicotine could activate the PI3K-Akt/PKB pathway or pathways and increased survival of mesencephalic dopaminergic cells against rotenone-induced cell death.

DISCUSSION

Rotenone works as a mitochondrial complex I inhibitor. Acute lethal doses of rotenone eliminate the mitochondrial respiratory system of the cell, resulting in an anoxic status that immediately causes cell death. At sublethal doses, it causes partial inhibition of mitochondrial complex I, and in this situation mitochondrial dysfunction leads to increased oxidative stress, decreased ATP production, increased aggregation of unfolded proteins, and then activated apoptotic pathway or pathways that result in cell death (Betarbet et al., 2000), resembling DA neurodegeneration in PD. Our data in vivo suggest that nicotine attenuated dopaminergic neuronal death of orally rotenone-treated PD model mice. It was relevant to the reports about the forebrain of rat models